VARIANCE REDUCTION IN A THREE-DIMENSIONAL SPACE USING THE CORRECTON METHOD

PNR-131-2011-001

M.V. Huisman

January 2011

Variance Reduction in a Three-Dimensional Space using the Correcton Method

Delft
January 2011

M.V. Huisman
Bachelor Applied Physics
1357964

Supervised by
ir. Bart Sjenitzer

Second Evaluator
dr.ir. Eduard Hoogenboom

Delft University of Technology
Faculty of Applied Sciences
department of
Radiation, Radionuclides & Reactors
section
Physics of Nuclear Reactors

Table of Contents

List of Figures

List of Tables

Abstract

This research project extents the correcton simulation technique in to an three-dimensional space. The correcton method is an hybrid Monte Carlo-deterministic technique for simulating global particle transport-problems. It couples a cheap deterministic calculation, with a more extensive Monte Carlo simulation. The estimated fluxes of the neutron flux are called the scalar flux guess, the particles used in the correcton methods are correctons. In this thesis various scalar flux guesses are compared.

The different methods are tested by looking at cube of 15x15x15 cm. This cube contains a source region in one of it is corners. First the flux shape is found using the analog Monte Carlo method. This method is time consuming and not precise. When a billion particles are used, the complete flux shape is not found.

The different flux guesses are compared in the cell that is the furthest away of the source, the value that is investigated is the Figure of Merit. This value gives an idea of the performance of the calculation. There are four different scalar fluxes guesses compared, namely 1-directional flux guess, 3-directional flux guess, discrete guess and adjoint flux guess

The first scalar flux guess that is made is an 1-directional flux guess in the x-direction. There are two kinds of guesses made, namely a strong and weak one. Both are able to penetrate the whole system. The weak estimation has Figure of Merit-value of $9.522 \cdot 10^{-5}$ and the strong estimation has a value $1.944 \cdot 10^{-3}$. The same is done for the three directional flux guess. The weak estimation has Figure of Merit-value of $6.833 \cdot 10^{-3}$ and the strong estimation has a value $4.619 \cdot 10^{-2}$.

The discrete guess is divided into pure the discrete values of the discrete guess and discrete guess itself. The discrete values scores a Figure of Merit-value of $1.853 \cdot 10^{-4}$ and the discrete guess of $2.673 \cdot 10^{-2}$. The last scalar flux guess is the adjoint flux guess. The discrete values of the adjoint flux guess scores a Figure of Merit-value of $3.429 \cdot 10^{-4}$ and the adjoint flux guess of $2.984 \cdot 10^{-2}$. This makes the adjoint flux guess best preforming discontinuous flux guess.

The best estimation of the neutron flux is with the strong estimation of the 3-directional flux guess. The reason for why it is preforming the best is that the flux guess needs less calculation steps for calculation a new position than the discontinuous flux guesses. Thereby making it ideal for homogeneous materials, the discontinuous flux guesses are more interesting for non-homogeneous materials.

Chapter 1

Introduction

The goal of this thesis is to show that it is possible to estimate the neutron flux using the correcton method in an $3D$ space. The correcton method is a way to implement a flux guess into the Boltzmann equation. The benefit of this method is that the Figure of Merit in the calculated neutron flux is higher than when using analog Monte Carlo simulation. In the paper of Becker [Becker et al, 2006] and the master thesis of Bart Sjenitzer [Sjenitzer, 2009] this method is proven to indeed increase the Figure of Merit of the calculated neutron flux in an $1D$ space. The situations that the correcton method is tested in are neutron transport and criticality calculations. In Chapter 3, also an $1D$ situation is made to show that the method indeed will decrease the variance. It is interesting to see if this also applies to an $3D$ space. The background of how the code is working is shown in chapter 2.

The new part of the research can be found in chapter 4 and 5. Becker suggested that the correcton method is also possible in an $3D$ space, but did not prove it in 2006. In his PhD thesis of 2009, Becker uses an adjoint flux guess for solving his $3D$ source-detector and source-region problem. Becker suggested in ideas for the future not to look only at the adjoint flux guess, but also at other distributions. In this thesis besides a discrete adjoint flux guess also continuous flux guesses and discrete flux guesses are used. The continuous flux guess can be divided in to two subsections, namely one directional flux guess and a three directional flux guess. The adjoint flux guess and the discrete flux guess are two subsections of the discontinuous flux guess

The system that is used is a cube of 15x15x15 cm with a small cube, 1 cm^3, as source region in a corner. To measure the effectiveness of the flux guesses the Figure of Merit is investigated, this is done in the opposite corner of the source, making it a classical source-detector problem.

Chapter 2

Background

2.1 Monte Carlo Simulation

2.1.1 History of Monte Carlo Simulation

The first systematic application [Jäckel et al, 2010] of statistical sampling in science was Enrico Fermi in the early 1930's. He used it to predict the results of experiments in relation to the properties of the neutron. After World War II, the Los Alamos National Laboratory developed a new computer, ENIAC. Stanislaw Ulam suggested that the ENIAC computer should be used for statistical sampling. Nicholas Metropolis dubbed the numerical technique "the Monte Carlo method". Together with Neumann, Ulam, Fermi and others the Monte Carlo simulation was further developed. The ENIAC computer could do about 5000 additions or 400 multiplications per second and occupied the size of a large room. Today every computer is able to run a Monte Carlo simulation program and much faster than in the old days.

2.1.2 Theory of Monte Carlo

Jäckel defines Monte Carlo as follows:

> *"A Monte Carlo method is any technique whose purpose it is to approximate a specific measure defined on a given domain by the aid of sampling according to a pre-determined distributional law."*

In this thesis a Monte Carlo method is used to estimate the neutron flux in several situations. The reason why Monte Carlo method is used for solving neutron transport equations is, because the different interactions of the particles are stochastic event and the problem can not be solved using a deterministic program.

2.1.3 Production of Random Numbers

When the random number generator is used on a computer, random number sequence is not totally random. The random number is made with a logarithm function, the function repeats itself over time. This period is in the order of 2^{46}. When the sequence walked through, it will start at the beginning. The randomness of the sequence is therefore not totally random, this phenomenon is called pseudo-random. The benefit of this is that the calculation can be repeated. The typical production of random numbers is in the range between 0 and 1.

2.1.4 Generating a Probability Distribution

When using Monte Carlo simulation, it is desirable to have any variable depending on an uniform distributed variable, ρ. The probability that a random number is

smaller for a certain value should be equal for both distributions [Sjenitzer, 2009].

$$P\left(x < \rho\right) = P\left(y < s\right) \tag{2.1}$$

The probability is in the range between 0 and 1. Eq. 2.1 can be rewritten as a cumulative distributions:

$$\int_{-\infty}^{\rho} g\left(x\right) dx = \int_{-\infty}^{s} f\left(y\right) dy \tag{2.2}$$

The left side of the equation is the uniform distribution between 0 and 1 and $f\left(y\right)$ is the distribution needed. For the uniform distribution becomes:

$$\int_{-\infty}^{\rho} g\left(x\right) dx = \rho \tag{2.3}$$

Eq. 2.2 now becomes:

$$\rho = \int_{-\infty}^{s} f\left(y\right) dy \tag{2.4}$$

In this way any distribution can be made with an uniform distribution.

2.2 Material Properties

2.2.1 Microscopic Cross Section

Microscopic cross section is the probability that a neutron-nuclear reaction will occur [Duderstadt et al, 1976]. Because the radius of a nucleus is in the order of 10^{-12} cm, the geometrical cross section is in the order of 1 $barn$. The microscopic cross section can be defined as:

$$\sigma = \frac{\left(R/N\right)}{I} \tag{2.5}$$

Where R is the rate that reactions occur per unit area, I is the intensity of the beam and N is the number of target atoms per unit area. The total microscopic

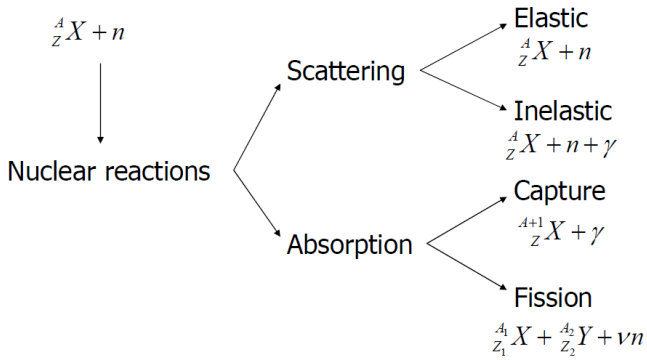

Figure 2.1: An overview of possible nuclear collision reactions.

cross section is sum of the individually microscopic cross section of the material. Therefore the total microscopic cross section becomes:

$$\sigma_t = \sigma_s + \sigma_c + \sigma_f \tag{2.6}$$

The subscript t is for the microscopic total cross section, s is for the scattering part, c is for the capture part and f is for the fission part. An overview of different reactions is shown if fig. 2.1 [Lathouwers et al, 2010].

2.2.2 Macroscopic Cross Section

The microscopic cross section is for small targets [Duderstadt et al, 1976], but a small target is not used in simulations. Instead a chunk of material is used, the macroscopic characterizes the probability of neutron interaction in that chunk. The macroscopic cross section is defined as:

$$\Sigma_i = N\sigma_i \tag{2.7}$$

Where N is the number density of nuclei in the target, which can be calculated with:

$$N = \frac{\rho_m N_A}{M_m} \tag{2.8}$$

Where ρ_m and M_m are the density and molar mass of the material and N_A is Avogadro constant (6.02214179 x 10^{23} mol^{-1})

2.3 Transport Equation for Monte Carlo Simulation

Neutron transport equation [Hoogenboom et al, 2008] in a stationary integro-differential form is defined as:

$$\begin{aligned}&\boldsymbol{\Omega}\cdot\nabla\phi\left(\mathbf{r},E,\boldsymbol{\Omega}\right)+\Sigma_t\left(\mathbf{r},E\right)\phi\left(\mathbf{r},E,\boldsymbol{\Omega}\right)=\\&\int_0^\infty\int_{4\pi}\Sigma_s\left(\mathbf{r},E'\rightarrow E,\boldsymbol{\Omega}'\rightarrow\boldsymbol{\Omega}\right)\phi\left(\mathbf{r},E',\boldsymbol{\Omega}'\right)dE'd\boldsymbol{\Omega}'+S\left(\mathbf{r},E,\boldsymbol{\Omega}\right)\end{aligned} \tag{2.9}$$

Where the variables $\mathbf{r}$, E and $\boldsymbol{\Omega}$ are for the position, energy and angle. The neutron flux is $\phi\left(\mathbf{r},E,\boldsymbol{\Omega}\right)$ and the source part is $S\left(\mathbf{r},E,\boldsymbol{\Omega}\right)$. The total and scatter macroscopic cross section are Σ_t and Σ_s. An apostrophe means the variable before the collision or the transition.

This equation is not suitable for Monte Carlo simulations because it is difficult to simulated. A better way is to think in terms of neutron events like the source, transitions and collisions. We define the source as:

$$S\left(\mathbf{r},E,\boldsymbol{\Omega}\right) \tag{2.10}$$

For the probability for a neutron to make a transition kernel is defined as:

$$T\left(\mathbf{r}'\rightarrow\mathbf{r},E,\boldsymbol{\Omega}\right)dV \tag{2.11}$$

and for the probability for a neutron to make a collision with exiting energy E and a direction $\boldsymbol{\Omega}$

$$C\left(\mathbf{r},E'\rightarrow E,\boldsymbol{\Omega}'\rightarrow\boldsymbol{\Omega}\right)dEd\boldsymbol{\Omega} \tag{2.12}$$

The last things to be defined are the event densities. The collision density is:

$$\psi\left(\mathbf{r},E,\boldsymbol{\Omega}\right) \tag{2.13}$$

and the emission density is:

$$\chi\left(\mathbf{r},E,\boldsymbol{\Omega}\right) \tag{2.14}$$

Now it is possible to deduce the following relations

$$\chi(\mathbf{r}, E, \mathbf{\Omega}) = S(\mathbf{r}, E, \mathbf{\Omega}) + \int_V T(\mathbf{r}' \to \mathbf{r}, E, \mathbf{\Omega}) \psi(\mathbf{r}, E, \mathbf{\Omega}) dV \quad (2.15)$$

$$\psi(\mathbf{r}, E, \mathbf{\Omega}) = \int_0^\infty \int_{4\pi} C(\mathbf{r}, E' \to E, \mathbf{\Omega}' \to \mathbf{\Omega}) \chi(\mathbf{r}, E', \mathbf{\Omega}') dE' d\mathbf{\Omega}' \quad (2.16)$$

To make it easier to read the previous two equation, a short-hand notation and a combined transport kernel will be defined:

$$(\mathbf{P}) = (\mathbf{r}, E, \mathbf{\Omega}) \quad (2.17)$$

$$L(\mathbf{P}' \to \mathbf{P}) = C(\mathbf{r}, E' \to E, \mathbf{\Omega}' \to \mathbf{\Omega}) T(\mathbf{r}' \to \mathbf{r}, E, \mathbf{\Omega}) \quad (2.18)$$

The Eq. 2.15, 2.16, 2.17 and 2.18 combined gives:

$$\psi(\mathbf{P}) = \int_V C(\mathbf{r}, E' \to E, \mathbf{\Omega}' \to \mathbf{\Omega}) S(\mathbf{r}', E, \mathbf{\Omega}) dV' + \int L(\mathbf{P}' \to \mathbf{P}) \psi(\mathbf{P}') d\mathbf{P}' \quad (2.19)$$

The next step is to split $\psi(\mathbf{P})$ into components where every component has had k collisions.

$$\psi(\mathbf{P}) = \sum_{k1=0}^{\infty} \psi_k(\mathbf{P}) \quad (2.20)$$

Where k is the number of collisions that had occur. When $k = 0$ collisions the source is given

$$\psi_0(\mathbf{P}) = \int_V C(\mathbf{r}, E' \to E, \mathbf{\Omega}' \to \mathbf{\Omega}) S(\mathbf{r}', E, \mathbf{\Omega}) dV' \quad (2.21)$$

The relationship between collision density around a collision is defined as:

$$\psi_k(\mathbf{P}) = \int \psi_{k-1}(\mathbf{P}') L(\mathbf{P}' \to \mathbf{P}) d\mathbf{P}' \quad (2.22)$$

This leads to:

$$\psi_k(\mathbf{P}) = \int ..... \int \psi_0(\mathbf{P_0}) \cdot K_0 \cdot K_1 .....K_{k-1} dP_0 .....dP_{k-1} \quad (2.23)$$

When the source is known of a reactor, the collision density can be calculated with Eq. 2.23. An overview of the path of a neutron is shown in Fig. 2.2. The way of modeling is discussed in the next section.

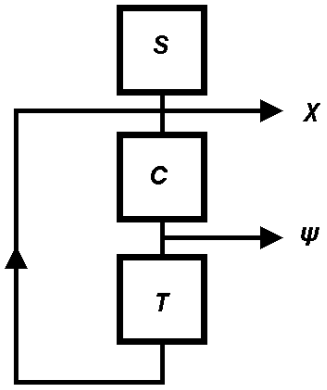

Figure 2.2: An overview of the path of a neutron, where S stands for the source, T for the transition and C for the collision. Also the collision density, χ, and emission density, ψ, are shown.

2.4 Modeling the Life of a Neutron

2.4.1 Transition

The distance that a neutron travels between two collision is a Poisson distribution [Sjenitzer, 2009]. It can be anywhere between 0 and ∞, but with the result of Eq. 2.4 it possible to calculate the travel distance:

$$\begin{aligned} \int_0^\rho d\rho' &= \int_0^s \Sigma_t e^{-\Sigma_t s'} ds' \\ \rho &= 1 - e^{-\Sigma_t s} \\ s &= -\frac{\ln(\rho - 1)}{\Sigma_t} \end{aligned} \tag{2.24}$$

The mean free path length is $\lambda = 1/\Sigma_t$. Because in this paper an $3D$ space will be used, the following two angles must be defined:

$$\begin{aligned} \mu &= 2\rho - 1 \\ \phi &= 2\pi\rho \end{aligned} \tag{2.25}$$

These two angles make up the the $3D$ space, these three angles are defined as:

$$\begin{aligned} u &= \mu \\ v &= \sqrt{1-\mu^2}\cos(\phi) \\ w &= \sqrt{1-\mu^2}\sin(\phi) \end{aligned} \tag{2.26}$$

Where u, v and w are the angle relative to the $\mathbf{\Omega}'$-axis, the $\mathbf{\Omega}'_{\perp\mathbf{1}}$-axis and the $\mathbf{\Omega}'_{\perp\mathbf{2}}$-axis, [Becker, 2009]. The $\mathbf{\Omega}'$-axis is the direction that a neutron got from the previous collision. The $\mathbf{\Omega}'_{\perp\mathbf{1}}$-axis and the $\mathbf{\Omega}'_{\perp\mathbf{2}}$-axis are orthogonal to the $\mathbf{\Omega}'$-axis. These sampled angles should be rotated to the canonical basis of $\mathbb{R}^3$, $\{\mathbf{i}, \mathbf{j}, \mathbf{k}\}$. The outgoing direction $\mathbf{\Omega}$ is defined as:

$$\mathbf{\Omega} = u \cdot \mathbf{\Omega}' + v \cdot \mathbf{\Omega}'_{\perp\mathbf{1}} + w \cdot \mathbf{\Omega}'_{\perp\mathbf{2}} \tag{2.27}$$

The collision is isotropic one and depends on the ingoing direction vector. Therefore the outgoing direction vector should be calculated as function of these variables. The basis should be rotated the canonical basis, where $\mathbf{\Omega}$ is represented as

$$\mathbf{\Omega} = \Omega_1\mathbf{i} + \Omega_2\mathbf{j} + \Omega_3\mathbf{k} \tag{2.28}$$

With this basis it is possible to calculated the new positions and the effective macroscopic cross section, Eq. 3.8. Where the basis vectors of Eq. 2.27 ate given by the following equations:

$$\mathbf{\Omega'} = \Omega'_1\mathbf{i} + \Omega'_2\mathbf{j} + \Omega'_3\mathbf{k} \tag{2.29}$$

$$\mathbf{\Omega'_{\perp 1}} = \frac{\Omega'_2}{\sqrt{\Omega'^2_1 + \Omega'^2_2}}\mathbf{i} - \frac{\Omega'_1}{\sqrt{\Omega'^2_1 + \Omega'^2_2}}\mathbf{j} \tag{2.30}$$

$$\mathbf{\Omega'_{\perp 2}} = \frac{\Omega'_1\Omega'_3}{\sqrt{\Omega'^2_1 + \Omega'^2_2}}\mathbf{i} + \frac{\Omega'_2\Omega'_3}{\sqrt{\Omega'^2_1 + \Omega'^2_2}}\mathbf{j} - \sqrt{\Omega'^2_1 + \Omega'^2_2}\mathbf{j} \tag{2.31}$$

The omegas with an apostrophe are the omegas of the incoming direction. The first event should be defined separately, because there is no previous direction vector.

$$\mathbf{\Omega} = u \cdot \mathbf{i} + v \cdot \mathbf{j} + w \cdot \mathbf{k} \tag{2.32}$$

The transition from the old position to the new position is given by:

$$\begin{aligned} x_{new} &= x_{old} + \Omega_1 \cdot s \\ y_{new} &= y_{old} + \Omega_2 \cdot s \\ z_{new} &= z_{old} + \Omega_3 \cdot s \end{aligned} \tag{2.33}$$

2.4.2 Sampling Collision

When a neutron has traveled a certain distance a collision occurs [Sjenitzer, 2009], with three possible events:

A capture event means that the neutron is absorbed in the material. The life of the neutron is therefore ended.

A fission event means that there are new neutrons made when the original neutron is captured by fissile material. On average ν new neutrons are produced, for good sampling not Σ_f is used but $\nu\Sigma_f$ in Eq. 2.34. The reason for this is that ν is not an integer number and it is desirable to have an integer number of new neutrons.

A scatter event means that the neutron will make collision with a nucleus and survives. It will get an new angle and it goes to the next collision.

The probability that one of the events has taken place is

$$\frac{\Sigma_i}{\Sigma_t} \tag{2.34}$$

Where i is a substitution for s, c and f. The subscript t is for the macroscopic total cross section, s is for the scattering part, c is for the capture part and f is for the fission part.

Implicit Capture

This method is also called survival biasing or survival by weight reduction. This method does not use a capture event, but it reduce the weight of the neutron. The weight lost is equal to the probability of capture. The new weight after a collision is:

$$wgt_{new} = wgt_{old}\left(1 - \frac{\Sigma_c}{\Sigma_t}\right) \tag{2.35}$$

If fission occurs it is also a form of absorption, therefore it is better to include this in the implicit capture:

$$wgt_{new} = wgt_{old}\left(1 - \frac{\Sigma_a}{\Sigma_t}\right) \tag{2.36}$$

This is called implicit absorption but implicit capture is also used for this equation. The drawback of this method is that the path of the neutron is only stopped when it is outside the system. Therefore it is useful to extend implicit capture with Russian roulette, because when the weight of the neutron is too small it has no added value to the calculation. Hence, when the weight becomes below a certain weight, wgt_{rr}, the change of survival is:

$$\frac{wgt}{wgt_{sur}} \tag{2.37}$$

If the neutron survivals the new weight is wgt_{sur}, in the model $wgt_{sur} = 2wgt_{rr}$ is used. On the other hand when the weight is to high you can split the neutron in two even parts with each half the weight.

2.4.3 Estimators

There are several estimators for the flux [Sjenitzer, 2009], but in this thesis only the collision estimator is used. The collision estimator is defined as:

$$\phi = \frac{1}{NV}\sum_{i}^{N}\left(\frac{wgt}{\Sigma_t}\right)_i \tag{2.38}$$

Where N is the number of particles, V is volume of the detector and for the summation a remark has to be made. A particle's score is the sum of all the scores for one estimator throughout it's lifetime. If the flux of the whole system desirable, multiple flux estimators are build in a regular structure.

2.5 Reduction of Variance

2.5.1 Statistics

When using the Monte Carlo simulation, it is important to know the variance of your answer. Due to the fact the found answer is only the estimation of the equation. There are two techniques [Dekking et al, 2003]: the law of large numbers and the central limit theorem.

The Law of Large Numbers

The law of large numbers tells that the mean of an estimation x is given by:

$$\mu = \lim_{N\to\infty}\frac{1}{N}\sum_{i=1}^{N} x_i \tag{2.39}$$

Where N is the number of particles, this is only valid when N is indeed ∞, then is μ a exact answer. But when $N < \infty$, the law of large numbers will not held up. Then the central limit theorem is needed.

The Central Limit Theorem

The estimated mean with the central limit theorem is given by:

$$\bar{x} = \frac{1}{N} \sum_{i=1}^{N} x_i \tag{2.40}$$

When the central limit theorem is used the found estimate mean is not precise. The variance is defined as:

$$s^2 = \frac{1}{N-1} \sum_{i=1}^{N} (x_i - \bar{x})^2 \tag{2.41}$$

Instead of using $\bar{x}$, it is also possible to fill in a theoretical value. Because the found estimate mean in equation 2.40 is not precise, the variance is desired. The variance of the mean is given by:

$$\begin{aligned} s^2_{\bar{x}} &= \frac{1}{N-1} \left(\frac{1}{N} \sum_{i=1}^{N} x_i^2 - \left(\frac{1}{N} \sum_{i=1}^{N} x_i \right)^2 \right) \\ s^2_{\bar{x}} &= \frac{1}{N} s^2 \\ \sigma_{\bar{x}} &= \sqrt{s^2_{\bar{x}}} \end{aligned} \tag{2.42}$$

In σ difference of the mean 68.2% of all answers can be found, for 2σ it is 95.5% and 99.7% for 3σ.

2.5.2 Principles of Variance Reduction

The reason why variance reduction is desirable, because low variance means that the found answer has more certainty. To compare the different techniques the Figure of Merit, FOM, is used. First the relative error is defined:

$$\mathrm{RE} = \frac{\sigma_{\bar{x}}}{\bar{x}} \tag{2.43}$$

The relative error, RE, tells you about the effectiveness of the calculation. Then Figure of Merit is defined as:

$$\mathrm{FOM} = \frac{1}{\mathrm{RE}^2 T} \tag{2.44}$$

The relative error is proportional to $1/\sqrt{N}$ and the time, T, is proportional to N. This makes Figure of Merit independent of N. A high Figure of Merit is desirable, this means a short calculation time or a reduction of the relative error must be achieved.

Chapter 3

Correcton Method

3.1 Transform Neutrons to Correctons

When a large system is used, the analog Monte Carlo simulation, will only perform well close to the source. In the deep parts the flux has dropped several orders of magnitude. When the standard analog Monte Carlo method is used the relative error will increase in those parts.

The correcton method is a technique for reducing the variance of the calculation in deep parts. The Monte Carlo particles used in the correcton method are called correctons. The correcton flux is the multiplicative correction to the deterministic flux. The method ensures that the correctons are more uniform distributed than the neutrons. This means that the variance far from the source should in theorem decrease and the correctons will reach deeper parts.

The simplest form of the correcton method is the one without angular biasing [Becker et al, 2006]. Also it is considered that the model is a mono-energetic, isotropic scattering deep-penetration problem driven by a localized source:

$$\mathbf{\Omega} \cdot \nabla \psi (\mathbf{r}, \mathbf{\Omega}) + \Sigma_t \psi (\mathbf{r}, \mathbf{\Omega}) = \frac{\Sigma_s}{4\pi} \int_{4\pi} \psi \left(\mathbf{r}, \mathbf{\Omega}'\right) d\mathbf{\Omega}' + \frac{S(\mathbf{r})}{4\pi} \ , \ \mathbf{r} \in V \tag{3.1}$$

$$\textit{boundary conditions: } \psi (\mathbf{r}, \mathbf{\Omega}) = 0 \ , \ \mathbf{r} \in \partial V \ , \ \mathbf{\Omega} \cdot \mathbf{n} < 0 \tag{3.2}$$

Where the variables $\mathbf{\Omega}$ and $\mathbf{r}$ are for the angle and location. Left side of the equation is the balance of neutron flying in and out of system at $(\mathbf{r}, \mathbf{\Omega})$. The right side will have interaction and therefore will have a new angle.

The correcton method is an estimation of the neutron flux. When an approximated (scalar) flux guess, $\hat{\phi}(\mathbf{r})$, is made and the correcton flux, $f(\mathbf{r}, \mathbf{\Omega})$, is found. The angular flux can be found with:

$$\psi (\mathbf{r}, \mathbf{\Omega}) = \frac{\hat{\phi}(\mathbf{r})}{4\pi} f (\mathbf{r}, \mathbf{\Omega}) \tag{3.3}$$

The flux guess is divided with a factor of 4π solid angle, because the flux guess is the flux summation over all angles. When Eq. 3.3 is substituted into Eq. 3.1, the following equation is the result:

$$\mathbf{\Omega} \cdot \nabla \left(\frac{\hat{\phi}(\mathbf{r})}{4\pi} f (\mathbf{r}, \mathbf{\Omega}) \right) + \Sigma_t \frac{\hat{\phi}(\mathbf{r})}{4\pi} f (\mathbf{r}, \mathbf{\Omega})$$

$$= \frac{\Sigma_s}{4\pi} \int_{4\pi} \frac{\hat{\phi}(\mathbf{r})}{4\pi} f \left(\mathbf{r}, \mathbf{\Omega}'\right) d\mathbf{\Omega}' + \frac{S(\mathbf{r})}{4\pi} \ , \ \mathbf{r} \in V \tag{3.4}$$

$$\textit{boundary conditions: } \frac{\hat{\phi}(\mathbf{r})}{4\pi} f (\mathbf{r}, \mathbf{\Omega}) = 0 \ , \ \mathbf{r} \in \partial V \ , \ \mathbf{\Omega} \cdot \mathbf{n} < 0 \tag{3.5}$$

Equations 3.4 and 3.5 can simplified to:

$$\begin{aligned} &\boldsymbol{\Omega}\cdot\nabla f\left(\mathbf{r},\boldsymbol{\Omega}\right)+\left[\Sigma_t+\boldsymbol{\Omega}\cdot\nabla\ln\hat{\phi}\left(\mathbf{r}\right)\right]f\left(\mathbf{r},\boldsymbol{\Omega}\right)\\ &\quad=\frac{\Sigma_s}{4\pi}\int_{4\pi}f\left(\mathbf{r},\boldsymbol{\Omega}'\right)d\boldsymbol{\Omega}'+\frac{S\left(\mathbf{r}\right)}{\hat{\phi}\left(\mathbf{r}\right)}\ ,\ \mathbf{r}\in V \end{aligned} \tag{3.6}$$

$$\textit{boundary conditions: } f\left(\mathbf{r},\boldsymbol{\Omega}\right)=0\ ,\ \mathbf{r}\in\partial V\ ,\ \boldsymbol{\Omega}\cdot\mathbf{n}<0 \tag{3.7}$$

The result of Eq. 3.6 looks quite similar to Eq. 3.1 only the total macroscopic cross section is different. The total macroscopic cross section in Eq. 3.6 is called the effective total macroscopic cross section and is defined as:

$$\Sigma_{t,\mathit{eff}}=\Sigma_t+\boldsymbol{\Omega}\cdot\nabla\ln\hat{\phi}\left(\mathbf{r}\right) \tag{3.8}$$

It is desirable that the effective total macroscopic cross section does not depend on the position of the particle and it must be positive all the time. The effective total macroscopic cross section will be put in the standard Monte Carlo simulation at the place of the total macroscopic cross section. For example the loss of weight will now be:

$$wgt_{new}=wgt_{old}\left(\frac{\Sigma_s}{\Sigma_t+\boldsymbol{\Omega}\cdot\nabla\ln\hat{\phi}\left(\mathbf{r}\right)}\right) \tag{3.9}$$

3.2 The System

The $1D$ system is a slab of 25 cm thick. The material has a total macroscopic cross section of 1 cm^{-1} and a macroscopic scatter cross section of 0.7 cm^{-1}. This means that the system 25 mean free paths deep is. To measure the neutron flux, 25 flux estimators are build every centimeter. The transport Eq. 3.1 becomes:

$$\begin{array}{ccccccc} \mu\frac{d\psi(x,\mu)}{dx}+\Sigma_t\psi\left(x,\mu\right) & = & \frac{\Sigma_s}{2}\int_{-1}^{1}\psi\left(x,\mu'\right)d\mu' & 0< & x & \leq 25\\ \psi\left(0,\mu\right) & = & 1 & 0< & \mu & \leq 1\\ \psi\left(25,\mu\right) & = & 0 & -1\leq & \mu & <0 \end{array} \tag{3.10}$$

The $\boldsymbol{\Omega}$ of Eq. 3.1 for the x direction is not taken from Eq. 2.26, but only the angle μ is used. After each collision a new angle μ is sampled and used for the effective total macroscopic cross section. The first boundary condition tells the system where the source is, the second indicates a vacuum at the right of the system.

3.3 Implementing Correctons

Because a exponential decay is expected, the flux can be estimated with:

$$\hat{\phi}\left(x\right)=2e^{-\beta x} \tag{3.11}$$

Because the flux is independent of the angle μ, a summation of the angles should be made, hence the factor 2. Where the estimation of the β is found with:

$$\begin{array}{rcl} \beta & = & \dfrac{\sqrt{3\left(1-c\right)}}{1+\left(\sqrt{3}-1\right)\left(1-c\right)}\\ c & = & \dfrac{\Sigma_s}{\Sigma_t} \end{array} \tag{3.12}$$

For this material $\beta \approx 0.77$. Using Eq. 3.8 the effective macroscopic cross section for this system becomes:

$$\Sigma_{t,eff} = \Sigma_t - \beta\mu \tag{3.13}$$

Because $\Sigma_t = 1$ and $|\mu| \leq 1$, the values for β should be in the range of $0 \leq \beta < 1$, otherwise a negative effective cross section is possible. The start weight is defined as:

$$wgt_{correcton} = \frac{1}{\hat{\phi}(\mathbf{r})} wgt_{neutron} \tag{3.14}$$

To transform the found correcton flux back to a neutron flux, the following equation will be used:

$$wgt_{neutron} = \hat{\phi}(\mathbf{r}')\, wgt_{correcton} \tag{3.15}$$

The transformation is done when a score is registered, but the weight of the particle stays in the correcton frame of reference when it travels futher in the system.

3.4 The Results

There are two estimations made, namely the estimated β value 0.77 and mid range $\beta = 0.39$. Also an analog Monte Carlo simulation is made using $\beta = 0$. The flux guess and the found analog neutron flux are plotted in Fig. 3.1.

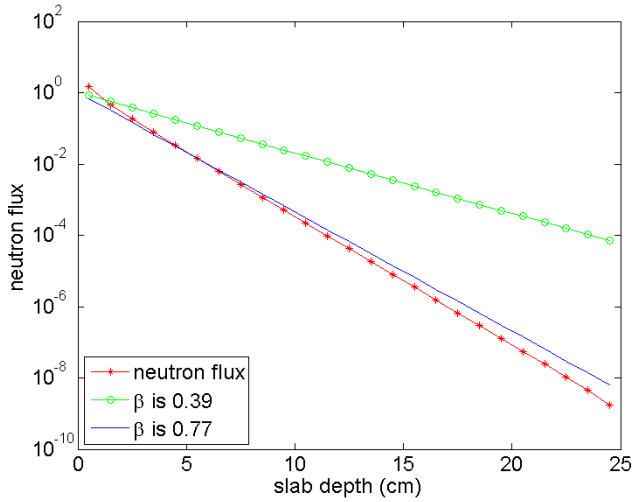

Figure 3.1: An overview of flux guesses and the neutron flux.

The neutron fluxes are plotted in Fig. 3.2, besides the flux also the error bars (1 $\sigma_{\bar{x}}$) are shown. The three found neutron fluxes are overlapping each other nice, but in the deeper parts the standard deviation of the analog Monte Carlo simulation is increasing. This happens because too few particles have reached this part of the system.

A better way to compare the different estimations is to look at the FOM, as explained in subsection 2.5.2. For Eq. 2.44 the time of calculating the neutron flux for one estimation is used. For the deep parts the relative error is smaller if the estimation becomes closer to the actual neutron flux. Because extra steps were made for

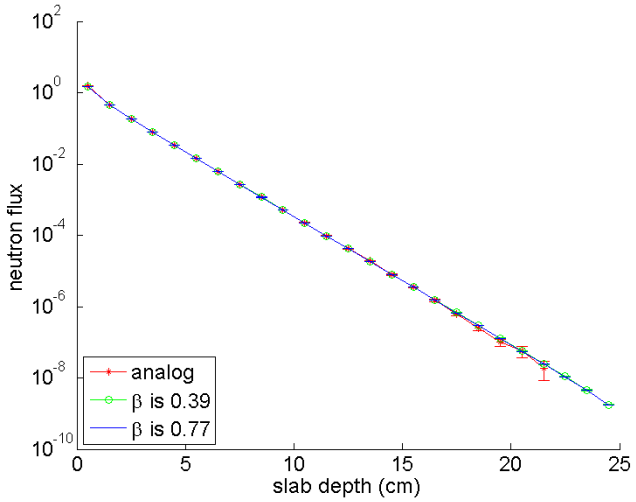

Figure 3.2: An overview of the neutron fluxes found for different β-values and by using the analog Monte Carlo method.

calculation the effective macroscopic cross section, the calculation time increases. Therefore there is a smaller FOM closer to the source, also the fact that the particles are now more even distributed throughout the system increases the relative error near the source. The conclusion is that the estimation using $\beta = 0.77$ gives a much more better result then the analog Monte Carlo simulation, but also $\beta = 0.39$ gives a better result.

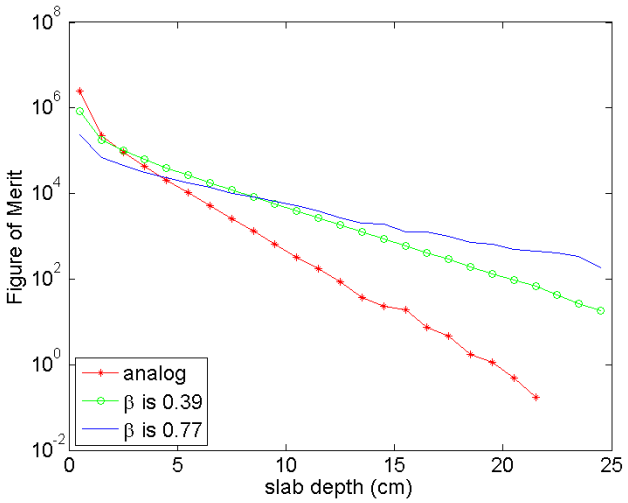

Figure 3.3: An overview of the FOM the analog Monte Carlo Simulation and the two flux guesses. The neutron flux can be found in Fig. 3.2.

Chapter 4

Extension of the Correcton Method to a 3D Environment

4.1 The System

The $3D$ system is a cube of 15x15x15 cm. The material is the same as in the $1D$ shielding problem, so it has a total macroscopic cross section of 1 cm^{-1} and a macroscopic scatter cross section of 0.7 cm^{-1}. Because the system is symmetric, it is only necessary to measure a plane. Also an $4D$, a position(x,y,z) and the neutron flux, plot hard to visualize. Therefore the flux through the x-plane, y-plane and the rear side (relative to the source) will be measured. The comparison is made by looking at the space diagonal. The source is defined as:

$$\begin{aligned} x &= \rho \\ y &= \rho \\ z &= \rho \\ \mu &= 2\rho - 1 \\ \phi &= 2\pi\rho \end{aligned} \tag{4.1}$$

Where ρ is a random number between 0 and 1. The start weight of a neutron is taken 1. The cube is placed in vacuum. Therefore once the neutron is outside the system, it will be lost.

4.2 Implementing Correctons

There are two flux guesses made. The first one is an 1-directional flux guess in the x-direction.

$$\hat{\phi}(\mathbf{r}) = 4\pi e^{-\beta x} \tag{4.2}$$

The flux guess is independent of the angles μ and ϕ, a summation of the angles should be made, hence the factor 4π. The estimation is plotted in Fig. 4.1. The estimated β of Eq. 3.12 can not be used because the neutrons have two more degrees of freedom, therefore a higher exponential decay is expected. Using Eq. 3.8 the effective macroscopic cross section for the flux guess becomes:

$$\Sigma_{t,\mathit{eff}} = \Sigma_t - \beta\Omega_1 \tag{4.3}$$

This effective macroscopic cross section is the same as for the $1D$ system, see Eq. 3.13. Therefore the same conditions for β are usable. In other words the value which β can take is between 0 and 1.

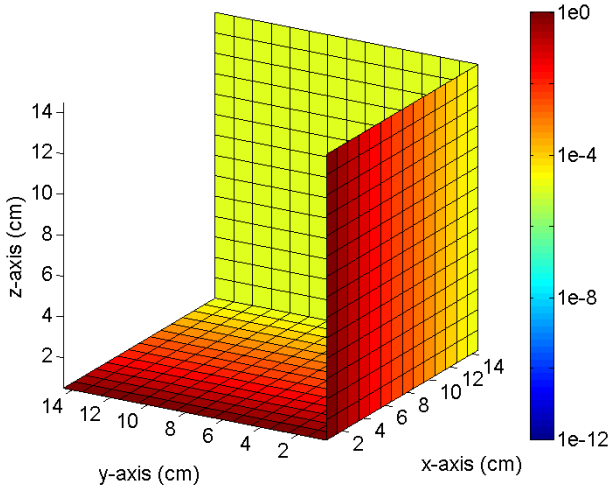

Figure 4.1: The 1-directional flux guess of Eq. 4.2 is plotted using the β-value 0.8.

The second flux guess is similar to the previous flux guess, but now a 3-directional flux guess is made. The assumption is made that in the x-, y- and z-direction the same decay factor (β) exists, because the material has homogeneous properties. This flux guess can be defined as:

$$\hat{\phi}\left(\mathbf{r}\right) = 4\pi e^{-\beta x} e^{-\beta y} e^{-\beta z} \tag{4.4}$$

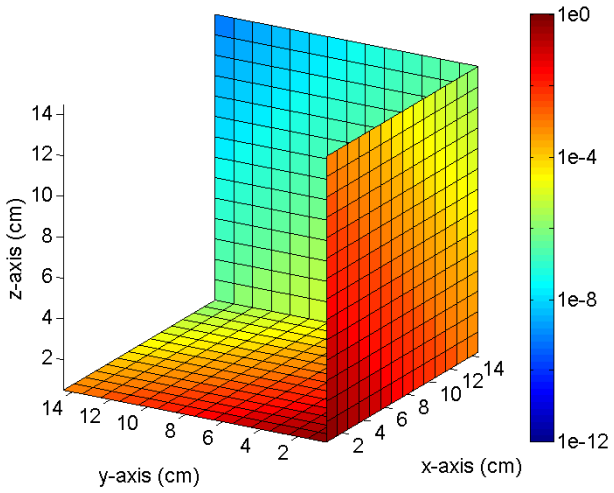

Figure 4.2: The 3-directional flux guess of Eq. 4.4 is plotted using the β-value 0.5.

This flux guess is also independent of the angles μ and ϕ, hence the factor 4π. The estimation is plotted in Fig. 4.2. Using Eq. 3.8, the effective macroscopic cross section becomes:

$$\Sigma_{t,\mathit{eff}} = \Sigma_t - \beta\left(\Omega_1 + \Omega_2 + \Omega_3\right) \tag{4.5}$$

First the maximum value of sum the angle is investigated. The sum of the begin

angles of Eq. 2.32, using Eq.2.26, looks like this:

$$\begin{gathered} u+v+w \\ \mu+\sqrt{1-\mu^2}\left(\cos(\phi)+\sin(\phi)\right) \end{gathered} \tag{4.6}$$

The ϕ-angle where the sum is the highest can be found at $\phi = \pi/4$. This value is inserted in the previous equation.

$$\begin{gathered} \cos(\pi/4)+\sin(\pi/4)=\sqrt{2} \\ \mu+\sqrt{2}\sqrt{1-\mu^2} \end{gathered} \tag{4.7}$$

The highest value for Eq. 4.7 is at $\mu = \sqrt{1/3}$. The sum of the angles has then a value of $\sqrt{3}$, because Σ_t has a value of 1 and the maximum β-value can be found:

$$\beta_{max} = \sqrt{1/3} \approx 0.57 \tag{4.8}$$

This value should not be exceeded otherwise a negative effective cross section is found.

4.3 The Results

The results are split into four subsections. The first three will contain a different estimation of the neutron flux. Because a $3D$ flux is difficult to visualize, three slice are made through the system. There are three planes chosen, see Fig. 4.3, which will be plotted. In the last subsection the neutron flux and the FOM is analyzed by looking at space diagonal of the system. For each simulation the same number of particles is used, namely 1 billion.

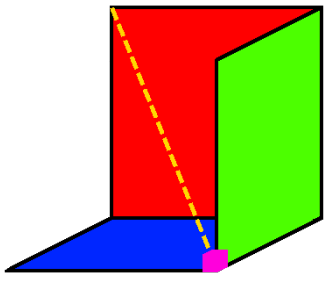

Figure 4.3: The pink cube is the source in the system. The blue plane, subfigures a, is the z-plane, the green plane, subfigures b, is the y-plane and the red plane, subfigures c, is the rear side of the system. The yellow dashed line is the line on which the different methods are compared.

4.3.1 The Analog Monte Carlo Simulation

In Fig. 4.4 the analog Monte Carlo is plotted. The analog Monte Carlo makes uses of implicit capture and Russian roulette, these techniques are also used when the flux guesses are made. This modified analog Monte Carlo is this thesis called the analog Monte Carlo simulations. The dark blue parts of the flux are parts where no neutrons are found. The model has also run with an higher number of particles, but the results is not the same as the result of a billion particles. The reason for this is that the program has not got a high enough precision. When using more then one billion particles it will be very time consuming, it is not strange to wait a day or two for the results and still the system is not well penetrated. This fact shows that the analog Monte Carlo method is not ideal for calculating the neutron flux in large areas. There is a clear circular pattern to see around the source. The explanation for this phenomenon is that an isotropic scattering is used, therefore the particles have no direction of preference. At the edges of the system a decrease of the flux is seen, this is because the system is placed in vacuum.

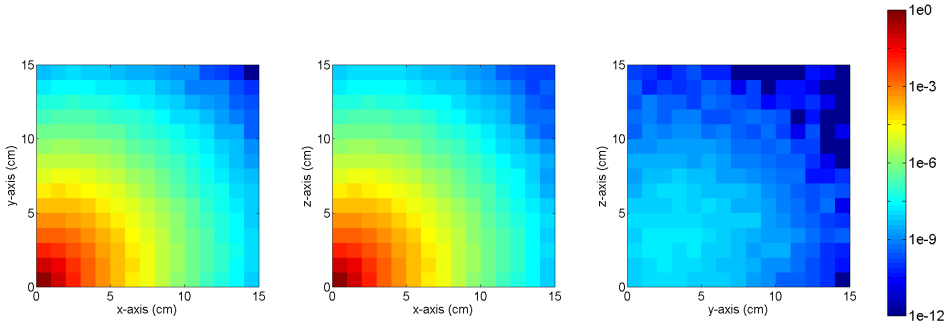

(a) z-plane (b) y-plane (c) the rear side

Figure 4.4: The found neutron flux using an analog Monte Carlo simulation.

When looked at the FOM, Fig. 4.5, the same pattern as the flux can be seen. The reason for this is that the neutron particles have macroscopic effective cross section which is equal to the total macroscopic cross section. Therefore it has no angular dependence.

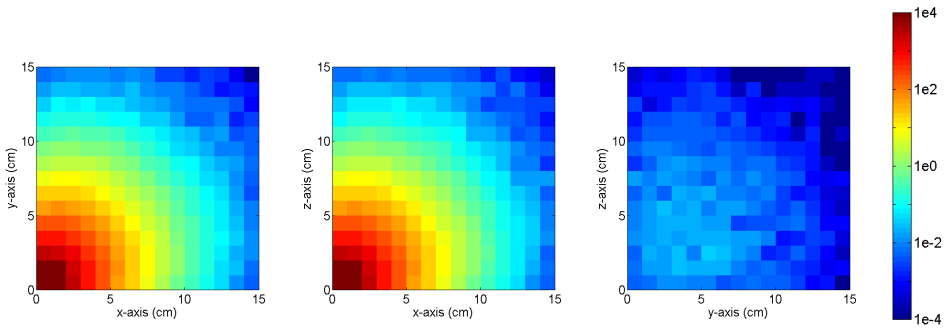

(a) z-plane (b) y-plane (c) the rear side

Figure 4.5: The FOM of the analog Monte Carlo simulation.

4.3.2 One Directional Continuous Flux Guess

At first a β-value is chosen which is higher than the estimated β-value calculated with Eq. 3.12. The optimal β-value for a $1D$ system is 0.77, the exponential decay factor for the $3D$ system is 0.8. This way the correctons have not a strong preference to move in the positive x-direction, otherwise the correctons will not reach to the y- and z-interfaces with the vacuum. The neutron flux is plotted in Fig. 4.6. At the rear side of the system a circular pattern is appears. The reason for this phenomenon is that the flux has a ratio with the distance with the source. The circles are positions where the distance are equal to each other, therefore the flux is the same.

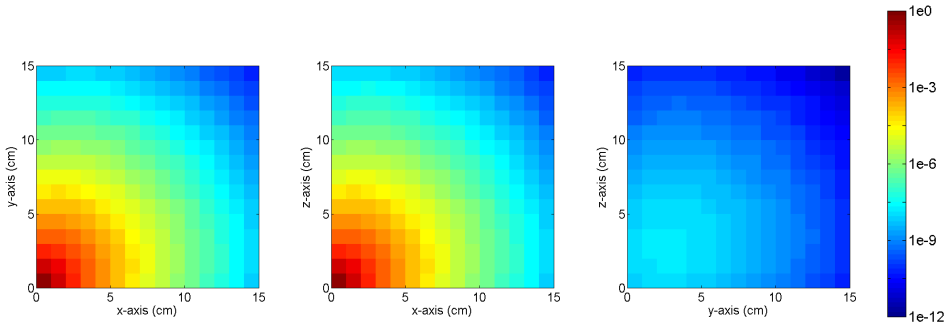

(a) z-plane (b) y-plane (c) the rear side

Figure 4.6: The neutron flux using an 1-directional flux guess, the chosen β-value is 0.8.

When the FOM, Fig. 4.7, is investigated the preference direction is clearly visible. The plane looks a lot like a smoke plume in the x-direction. In spite of using the 1-directional flux guess the FOM decreases slower than the analog Monte Carlo simulation.

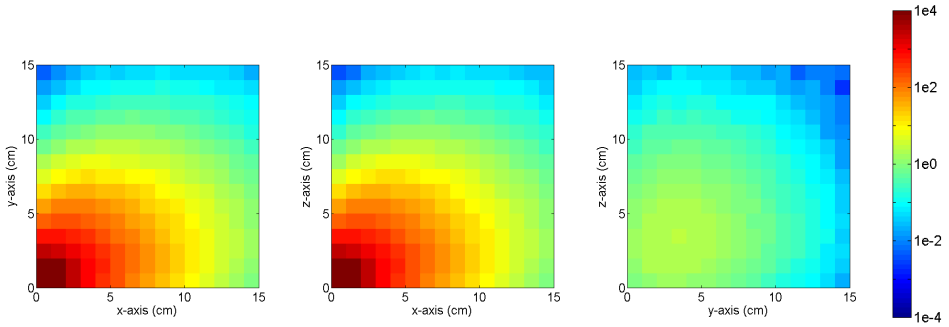

(a) z-plane (b) y-plane (c) the rear side

Figure 4.7: The FOM using an 1-directional flux guess, the chosen β-value is 0.8.

The same is done for a smaller β-value, namely 0.4. This value between the analog Monte Carlo simulation and β-value 0.8. This is done to show that a weak estimation also improves the found results. The results of the neutron flux, Fig. 4.8, are similar the results of the previous estimation, Fig. 4.6.

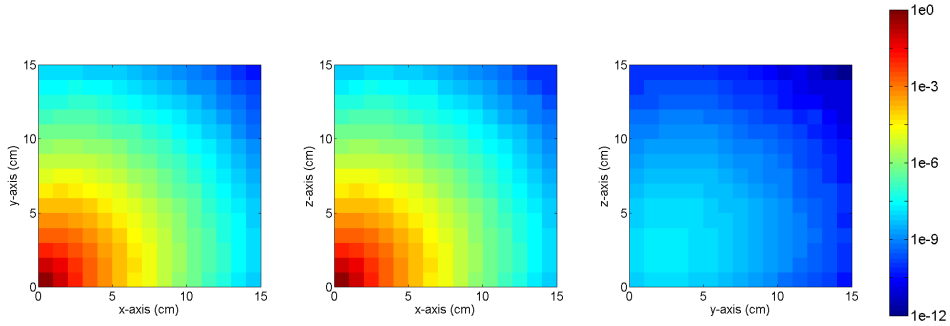

(a) z-plane (b) y-plane (c) the rear side

Figure 4.8: The neutron flux using an 1-directional flux guess, the chosen β-value is 0.4.

The FOM, Fig. 4.8, of this estimation has a smaller smoke plume as Fig. 4.11. The particles are now traveling less in the x-direction, the relative error increases in the deep parts. Hence the decrease of the FOM.

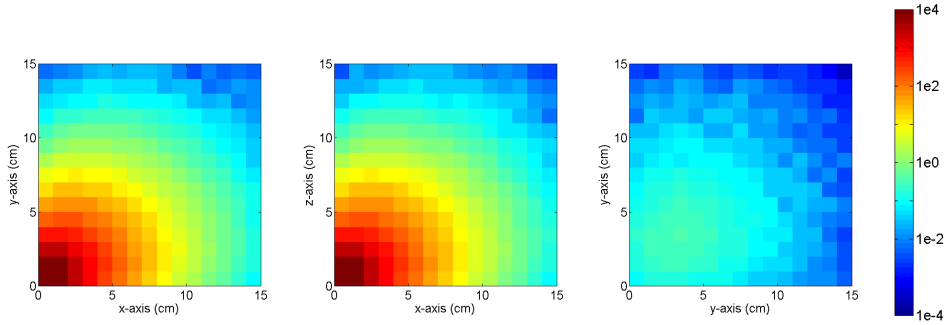

(a) z-plane (b) y-plane (c) the rear side

Figure 4.9: The FOM using an 1-directional flux guess, the chosen β-value is 0.4.

4.3.3 Three Directional Continuous Flux Guess

The neutron flux of a three directional flux guess is plotted in Fig. 4.10. The β-value is chosen to be 0.5, this is close to the maximum value, see Eq. 4.8.

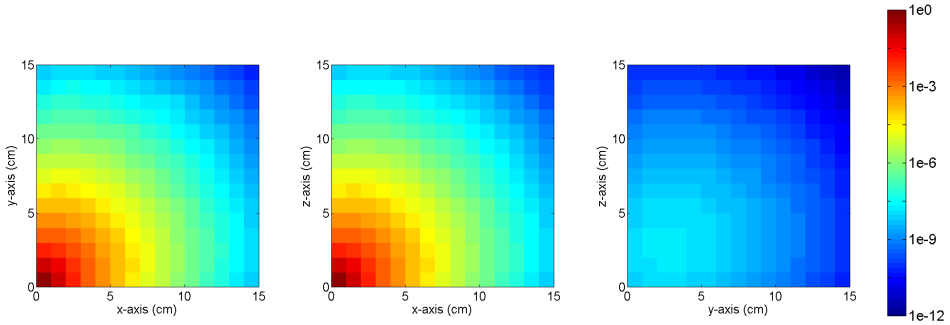

(a) z-plane (b) y-plane (c) the rear side

Figure 4.10: The neutron flux using an 3-directional flux guess, the chosen β-value is 0.5.

The value is chosen as high as possible, but not too close the maximum value, otherwise a distance can be sampled which is greater than the system. Because the particles have now a more uniform movement outwards from the source. The found structure of the flux in Fig. 4.10(c) is finer then that in Fig. 4.6(c).

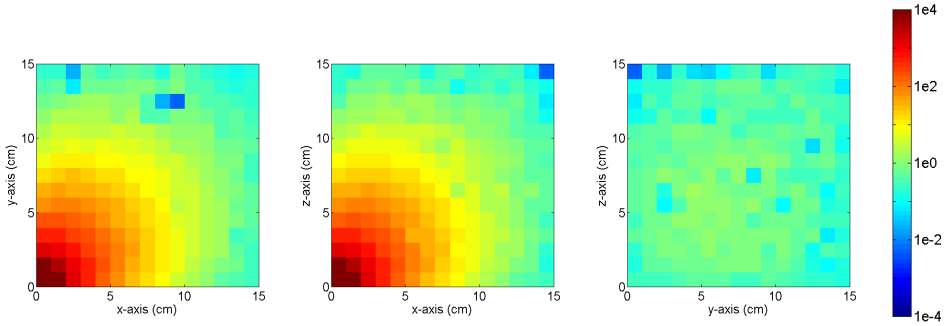

(a) z-plane (b) y-plane (c) the rear side

Figure 4.11: The FOM using an 3-directional flux guess, the chosen β-value is 0.5.

The FOM, Fig. 4.11, shows that the particles have equal preference in each direction. The spots mean that these cells are under sampled.

Just like the 1-directional flux guess a weaker estimation is made. This time the β-value is chosen between the strong estimation and the analog Monte Carlo Method, namely $\beta = 0.25$. The found neutron flux is just as fine as the strong estimation of the 3-directional flux guess.

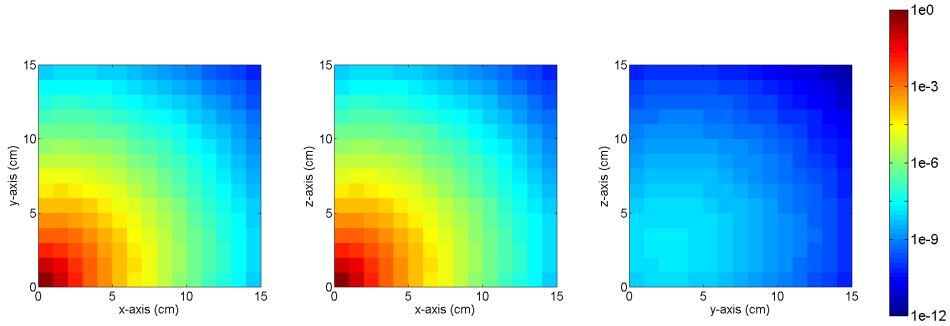

(a) z-plane (b) y-plane (c) the rear side

Figure 4.12: The neutron flux using an 3-directional flux guess, the chosen β-value is 0.25.

In Fig. 4.13 is the same phenomenon visible as in Fig. 4.11, but there is clear difference in the values of the FOM. This is also seen Fig. 4.18, where the two FOM lines are close to each other. Note that in Fig. 4.13 no spots are visible, apparently the β-value of 0.5 is too close to the maximum β-value causing a distance sampled greater than the cube.

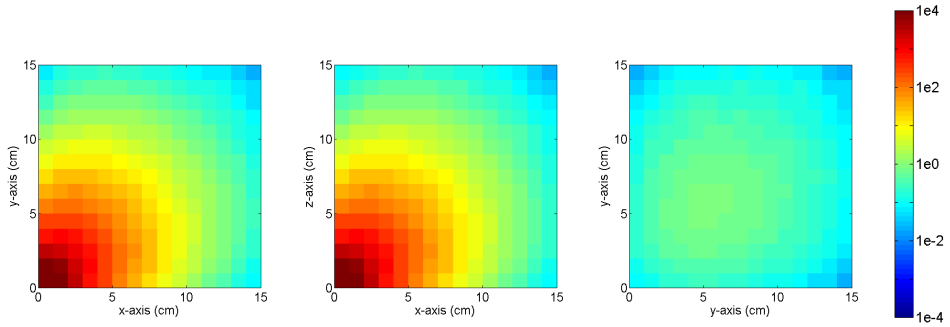

(a) z-plane (b) y-plane (c) the rear side

Figure 4.13: The FOM using an 3-directional flux guess, the chosen β-value is 0.25.

4.4 Comparison of the Found Results

As said the comparison is made at the space diagonal of the cube. The reason for that is the previous $2D$ plots does not show if the found neutron fluxes are within one $\sigma_{\bar{x}}$ of each other. First, an overview the estimations in Fig. 4.14 is seen.

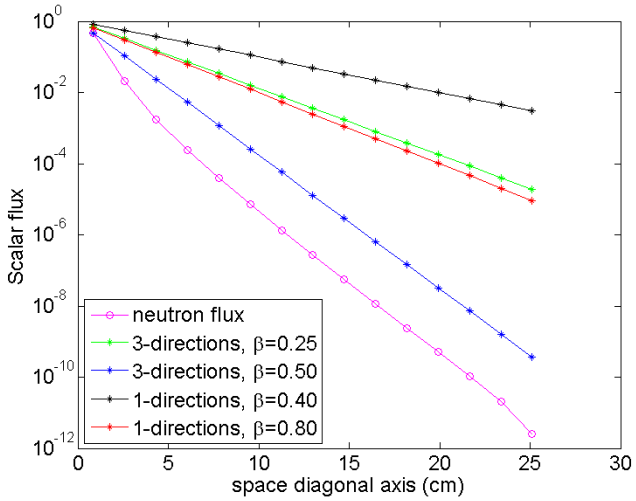

Figure 4.14: An overview of the 1- and 3-directional flux guesses and the found neutron flux.

In Fig. 4.15 the neutron fluxes are plotted using an one directional flux guess and the analog Monte Carlo simulation, also error bars (size is one $\sigma_{\bar{x}}$) are plotted. All found neutron fluxes are within these error bars, meaning they do not contradict with each other. The bend close to the source is due the fact a region source is used. Deeper in the system the source can be seen as a point source, hence the straight line. The fact that the analog Monte Carlo simulation is not reaching the deep part is visible and the weak estimation, $\beta = 0.4$, suffers from not having enough particles in deep parts.

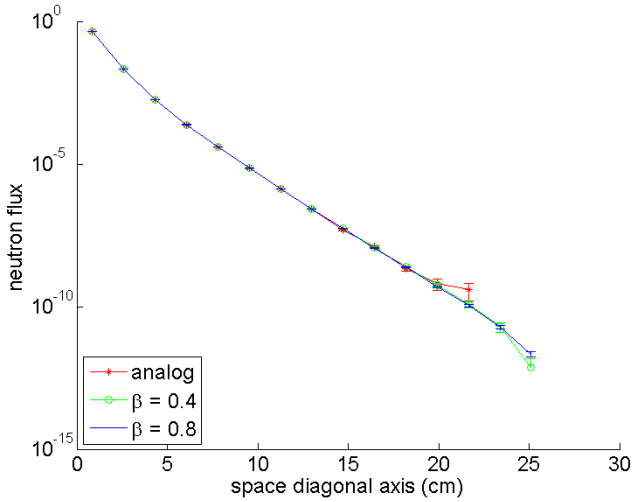

Figure 4.15: The neutron flux calculated using the 1-directional flux guess and the analog Monte Carlo Method.

The FOM of the neutron fluxes, Fig. 4.16, shows that the flux guesses have an higher FOM throughout the system. This means that the flux guesses preform better than the analog Monte Carlo method. Also the correctons are going deeper into the system.

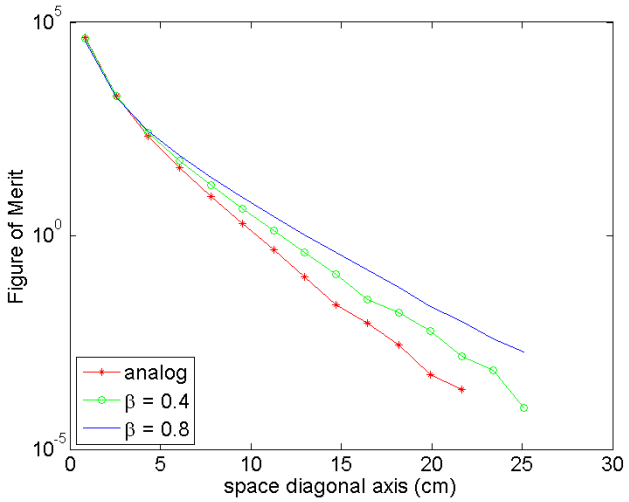

Figure 4.16: The FOM of the 1-directional flux guesses and the analog Monte Carlo Method.

The same plot as Fig. 4.15 is also done for the 3-direction flux guess, Fig. 4.17. In this plot the data points are also within one time the standard deviation of the mean. Both flux guesses are reach the deepest part of the cube with enough particles, which is good.

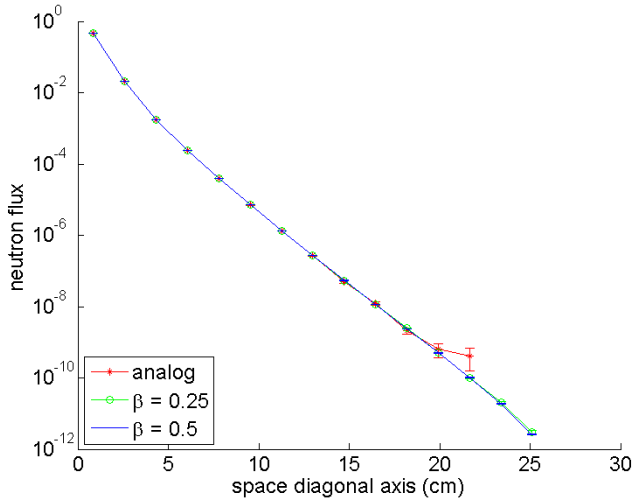

Figure 4.17: The neutron flux calculated using the 3-directional flux guesses and the analog Monte Carlo Method.

When the FOM, Fig. 4.18, is plotted of the methods of Fig. 4.17. It's clear to see that the estimations are preforming much better than the analog Monte Carlo method. Near the source a drop is seen caused by the longer processor time and the fact that the particle are more evenly distributed.

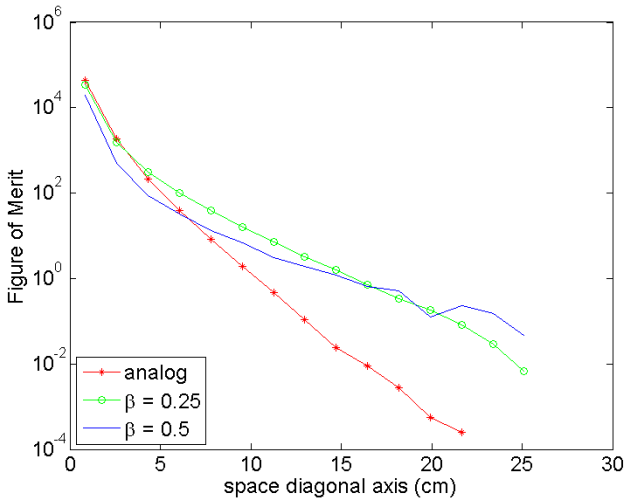

Figure 4.18: The FOM of the 3-directional flux guesses and the analog Monte Carlo Method.

To compare better the results, a closer look is taken at the furthest bin from the source. The data of this approach are shown in table 4.1 and 4.2.

Table 4.1: An overview of the results of the one directional flux guess in the opposite corner cell in comparison to the source.

Method	β-value	FOM	Time needed	Variance	Number of particles
Dimension		$-$	Hours	$\#^2\text{cm}^{-6}\text{s}^{-1}$	#
Analog		n.a.	2.8	n.a.	10^9
Weak estimation	$\beta = 0.40$	$9.522 \cdot 10^{-5}$	2.9	$5.828 \cdot 10^{-25}$	10^9
Strong estimation	$\beta = 0.80$	$1.944 \cdot 10^{-3}$	3.0	$2.307 \cdot 10^{-25}$	10^9

Table 4.2: An overview of the results of the three directional flux guess in the opposite corner cell in comparison to the source.

Method	β-value	FOM	Time needed	Variance	Number of particles
Dimension		$-$	Hours	$\#^2\text{cm}^{-6}\text{s}^{-1}$	#
Analog		n.a.	2.8	n.a.	10^9
Weak estimation	$\beta = 0.25$	$6.833 \cdot 10^{-3}$	3.2	$1.112 \cdot 10^{-25}$	10^9
Strong estimation	$\beta = 0.50$	$4.619 \cdot 10^{-2}$	3.5	$1.182 \cdot 10^{-26}$	10^9

It is not possible to compare the correcton method with the analog Monte Carlo method by looking at the tables, but the figures 4.16 and 4.18 shows that the analog method is not preforming better. To reach a complete penetration of the system by using the analog Monte Carlo simulation, an 100 times more particles should probably be used, which will cost roughly 12 days to calculated. The time difference between the two techniques is explained by the fact that the three directional flux guess has more calculation steps. When a look is taken at the column FOM, the best estimation of these four is the three directional flux guess with a β-value of 0.5. The effectiveness of a good estimation is good visible between the strong estimation of the one directional flux guess and the weak estimation of the three directional flux guess. The difference of the estimated flux is small, see Fig. 4.14, but the three directional flux guess is preforming much better. Because the one directional flux guess gives the particles a preference to move along the x-axis and the three directional flux guess gives the particles a more even distribution throughout the system.

Chapter 5

Correcton Method using Discrete and Adjoint Flux Guess

5.1 Discrete Flux Guess

5.1.1 Discretization of the Flux Guess

By discretization the flux guess a flux guess can made for each cell separately. The benefit is that the flux guess is prepared for using a non-homogeneous material. The flux guess is defined as:

$$\hat{\phi}(\mathbf{r}) = Ce^{-\beta_x \cdot (x-x_c)} e^{-\beta_y \cdot (y-y_c)} e^{-\beta_z \cdot (z-z_c)} \tag{5.1}$$

Where C is the amplitude of the scalar flux at the center of a bin. The center of the bin is defined as (x_c, y_c, z_c). Instead of using one β for all the directions, a β-value is calculated in each direction. The idea is to use a "cheap" method to estimate the scalar flux. The β-values for cell $C_{i,j,k}$ can be calculated using these equations:

$$\begin{aligned} \beta_{c,x} &= \frac{1}{\Delta x_i} \ln\left(\frac{\Phi_{i+1/2,j,k}}{\Phi_{i-1/2,j,k}}\right) \\ \beta_{c,y} &= \frac{1}{\Delta y_j} \ln\left(\frac{\Phi_{i,j+1/2,k}}{\Phi_{i,j-1/2,k}}\right) \\ \beta_{c,z} &= \frac{1}{\Delta z_k} \ln\left(\frac{\Phi_{i,j,k+1/2}}{\Phi_{i,j,k-1/2}}\right) \end{aligned} \tag{5.2}$$

Where Φ is the cheap estimation of the neutron flux. The flux is taken at the center points of the opposite faces. When the β-values are calculated using Eq. 5.2, they are checked if they are not causing a negative effective total macroscopic cross section. To this assumption is made that Ω_1, Ω_2 and Ω_3 have each a maximum at the same time, which is one. This theoretical is not possible, because of the interrelationships of the angles, see also Eq. 4.8. Still this assumption is used, therefore sum of the three β-values should not be greater then 1, if they are greater than one each β-value should be divided by the sum of the β-values, to keep the proportion between the β-values the same. When the continuous flux guess is used in the discontinuous code, the sum of the β-values can be greater, because the β-values are the same. In discrete model β-values are not the same amplitude to ensure that there will be no negative effective cross section this assumption is made

5.1.2 Discontinuous Flux Guess

The flux guess will be discontinuous when the sum of the decay factors are greater than one. Therefore some adjustments should be made to the weight of a particle at these discontinuities. Taken in mind that the neutron flux is continuous at the location of the discontinuous scalar flux guess.

$$\lim_{\epsilon \downarrow 0} \psi\left(\boldsymbol{r} + \epsilon\boldsymbol{\Omega}, \boldsymbol{\Omega}\right) = \lim_{\epsilon \uparrow 0} \psi\left(\boldsymbol{r} + \epsilon\boldsymbol{\Omega}, \boldsymbol{\Omega}\right) \tag{5.3}$$

In the previous equation is the definition of Eq. 3.3 substituted, the result is:

$$\frac{1}{4\pi} \lim_{\epsilon \downarrow 0} \hat{\phi}^{+}\left(\boldsymbol{r} + \epsilon\boldsymbol{\Omega}, \boldsymbol{\Omega}\right) \mathbf{f}^{+}\left(\boldsymbol{r} + \epsilon\boldsymbol{\Omega}, \boldsymbol{\Omega}\right) = \frac{1}{4\pi} \lim_{\epsilon \downarrow 0} \hat{\phi}^{-}\left(\boldsymbol{r} + \epsilon\boldsymbol{\Omega}, \boldsymbol{\Omega}\right) \mathbf{f}^{-}\left(\boldsymbol{r} + \epsilon\boldsymbol{\Omega}, \boldsymbol{\Omega}\right) \tag{5.4}$$

Here $\hat{\phi}^{-}$ is the old flux guess and $\hat{\phi}^{+}$ is the new flux guess. The smallest limit of the correcton flux is the weight of a single particle, therefore the the Eq. 5.4 is transformed to:

$$\left[\lim_{\epsilon \downarrow 0} \hat{\phi}^{+}\left(\boldsymbol{r} + \epsilon\boldsymbol{\Omega}, \boldsymbol{\Omega}\right)\right] wgt^{+} = \left[\lim_{\epsilon \downarrow 0} \hat{\phi}^{-}\left(\boldsymbol{r} + \epsilon\boldsymbol{\Omega}, \boldsymbol{\Omega}\right)\right] wgt^{-} \tag{5.5}$$

Now it is possible to calculate the new weight of the particle when it crosses a discontinuity in the flux guess.

$$wgt^{+} = wgt^{-} \frac{\hat{\phi}^{-}\left(\boldsymbol{r}\right)}{\hat{\phi}^{+}\left(\boldsymbol{r}\right)} \tag{5.6}$$

When a particle comes to a discontinuity in the flux guess, it is stopped. The particles weight is changed and a new distance is sampled. Note, the particle must still be stopped at the edges of the cell, because the β-values are different and therefore the effective total macroscopic cross section is different

5.1.3 The Estimation for the Discrete Flux Guess

The same system as in the previous chapter is used, meaning a cube of 15x15x15 cm with a small source cube in one of the corners. When the neutron flux is wanted at a great distance from the source, the source can be assumed to be a point source. The one-speed diffusion model gives a solution for an point source in an infinity medium. This solution is defined as:

$$\hat{\phi} = \frac{3\Sigma_t S_0}{4\pi} \frac{1}{r} e^{-r/L} \tag{5.7}$$

Where S_0 is the source strength, r is the distance to the source

$$r^2 = x^2 + y^2 + z^2 \tag{5.8}$$

and L is the diffusion length defined as:

$$L^2 = \frac{1}{3\Sigma_t \Sigma_a} \tag{5.9}$$

For the estimation the first fraction (Eq. 5.7) set to the value 1 and the point source is placed at the origin of the system. The amplitude of the center of the bins is plotted in Fig. 5.1. The neutron flux has the shape as found flux in the previous chapter. This estimation is not perfected, because it assumes a point source, but it is a source region. Also the fact that the cube is placed in vacuum is not accounted for.

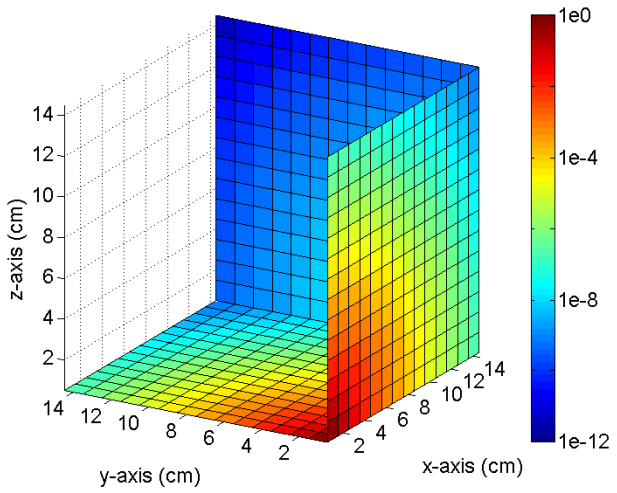

Figure 5.1: The neutron flux calculated with the diffusion theory for a source point in an infinite medium.

The β-values are plotted in Fig. 5.2. The β-values in the x-direction is the highest along the x-axis, because the distance relative to the source changes the most in this direction. Therefore a does have a little difference in the y and z direction.

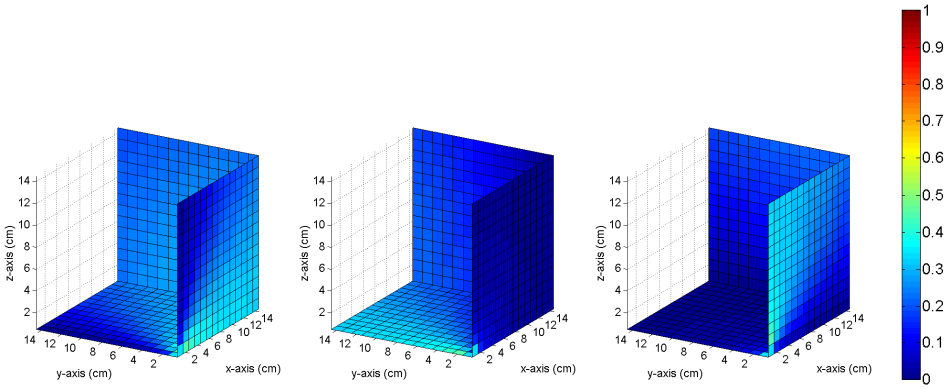

(a) x-direction (b) y-direction (c) z-direction

Figure 5.2: The different β-values in each direction after "normalization".

5.1.4 The Results

Discrete Flux Guess only with the Discrete Values of the Estimation

At first only the discrete values of the diffusion solution are used for making the estimation. This is done to show that the result improves by using this technique. The effect is that the particles weight is changing when it traveling through the cell boundary, the Russian roulette becomes a weight window. The found neutron flux, see Fig. 5.3, has the shape as the previous found neutron fluxes. But the particles are traveling deeper in the system because they gain weight, however the Russian roulette boundary is still the same. This leads to the fact that the deep parts have less "noise".

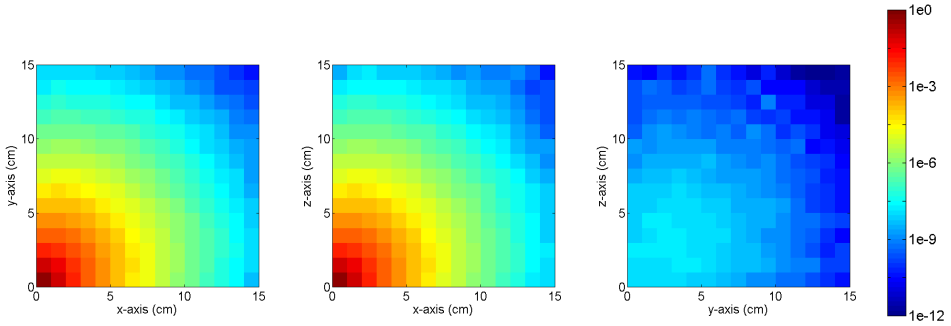

(a) z-plane (b) y-plane (c) the rear side

Figure 5.3: The neutron flux calculated using the discrete values of the discrete flux guess.

The FOM of Fig. 5.3 has the same shape as the analog Monte Carlo simulation, Fig. 4.5. This flux guess is preforming better than the analog Monte Carlo method, because the weight is changing throughout the system and the Russian roulette is a weight window. By doing so the particles have a longer lifetime and therefore penetrating the system better than the analog Monte Carlo method.

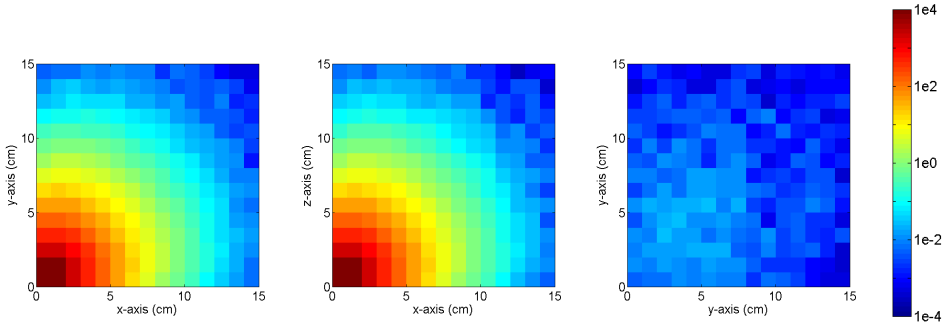

(a) z-plane (b) y-plane (c) the rear side

Figure 5.4: The FOM calculated using the discrete values of the discrete flux guess.

Discrete Flux Guess

The next step to implement the found β-values found by using Eq. 5.2. The benefit is that the effective total macroscopic section can be used, which will improve the distribution of the particles. As shown in the previous chapter this has a positive effect on the results. The neutron flux in Fig. 5.5 shows a neutron flux which is well defined, this is seen when a look is taken at the rear side of the system. The neutron flux has not got a blocky appearance as in Fig. 5.3, but is more smooth.

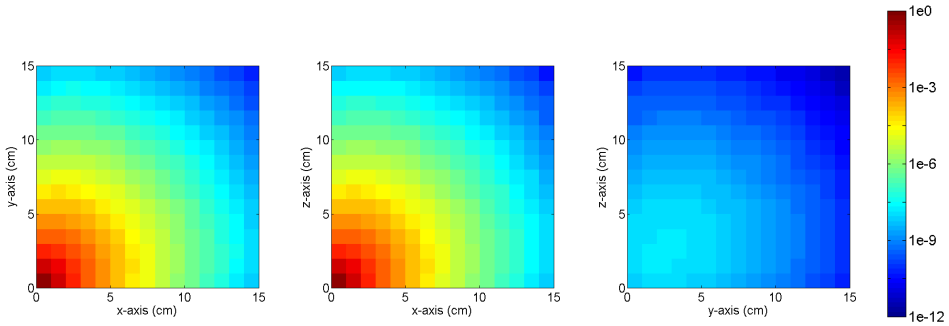

(a) z-plane (b) y-plane (c) the rear side

Figure 5.5: The neutron flux calculated using the discrete flux guess.

This is supported when a look is taken at the FOM, Fig. 5.6. The FOM is the first one where the values not coming below the 10^{-2}, this means that the calculation is going well, due to the fact that the particles are even more evenly distributed. The shape in Fig. 5.6(a) can be explained by the fact the particles are pushed along the "$\phi = \pi/4$"-line, at this line there is maximum for the sum of the angles. The shape in Fig. 5.6(b) is the effect that the particles are only traveling upwards in the system, this can also be seen at the rear side. There are the lower bins lesser sampled, hence the darking of color blue.

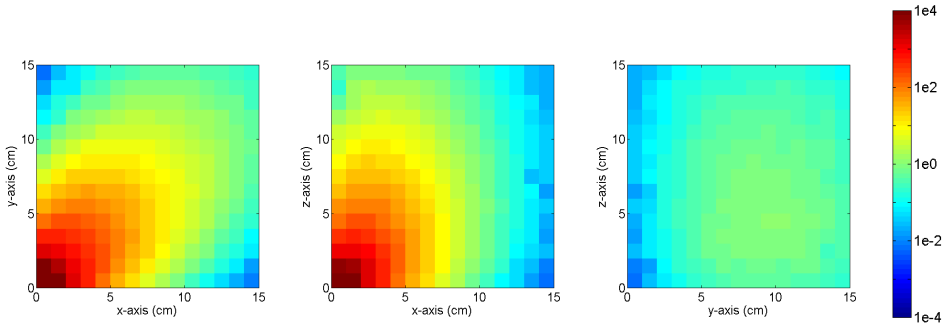

(a) z-plane (b) y-plane (c) the rear side

Figure 5.6: The FOM calculated using the discrete flux guess.

5.1.5 Comparison of the Found Results

Just like the previous comparisons a closer look is taken at the space diagonal, in this way the results can be more quantized. In Fig. 5.7 the neutron flux and the two flux guesses are plotted. These flux guesses stay closer to the real neutron flux than the continues flux guesses of Fig. 4.14.

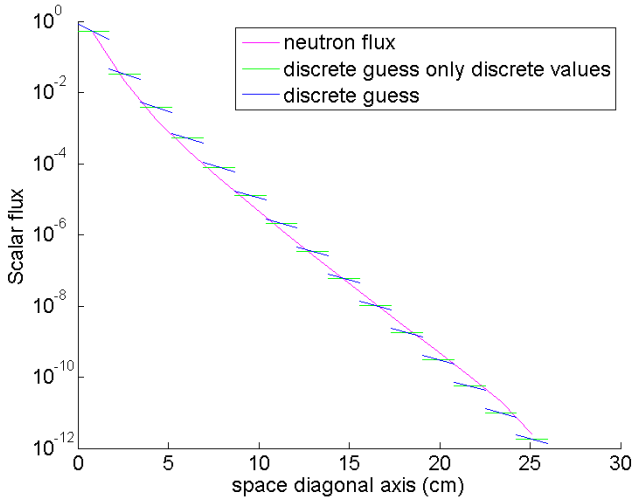

Figure 5.7: An overview of the discrete flux guess with only discrete values, discrete flux guess and the found neutron flux.

Close to the source the guess is not perfect but deeper in the system is it a good fit. Using the two flux guesses the neutron flux is calculated, see Fig. 5.8.

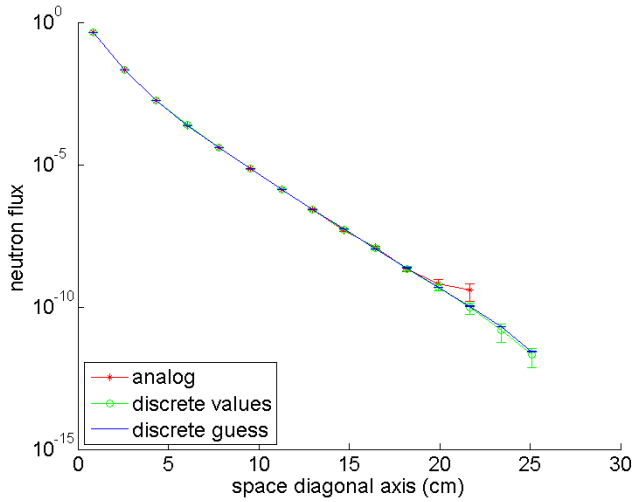

Figure 5.8: The neutron flux calculated with the discrete flux guess with only discrete values, discrete flux guess and analog Monte Carlo method.

The three found neutron fluxes are not contradicting each other, see Fig. 5.8 (plotted with error bars of one $\sigma_{\bar{x}}$). When a look is taken at the FOM, Fig. 5.9, it is seen that the discrete value are performing slightly better than the analog method. The

discrete guess is behaving much better that the analog Monte Carlo simulation.

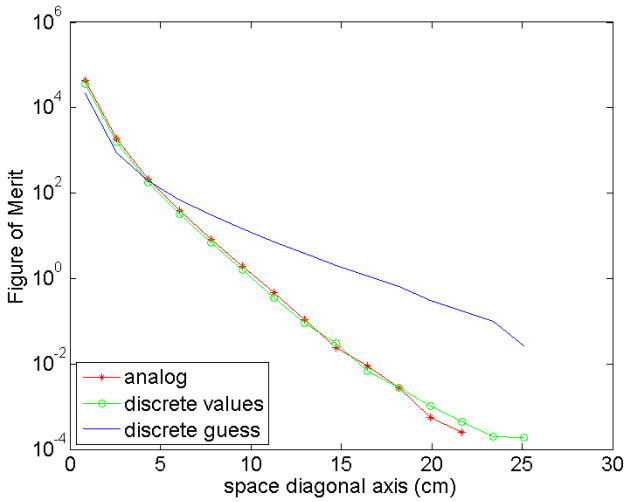

Figure 5.9: The FOM of the discrete flux guess with only discrete values, discrete flux guess and analog Monte Carlo method.

5.2 Adjoint Flux Guess

5.2.1 The Estimation for the Adjoint Flux Guess

In the end the results are compared by looking at the opposite corner, the so called detector. The adjoint flux guess is used an importance function or contribution flux. The importance function will tell which parts will score the most in the detector. The aim is that the particles are now have the tendency to move towards the detector. Through this process the detector will register more scores, thereby decreasing the relative error and in the end increasing the FOM. The last step will only occur when no extra time is needed. The adjoint flux guess can be founded using:

$$\psi\left(\mathbf{r}\right) = \frac{1}{\psi^{*}\left(\mathbf{r}\right)} \tag{5.10}$$

Where $\psi^{*}\left(\mathbf{r}\right)$ is the importance function. The result of this transformation only needs to take one more step and that is to normalize the amplitudes.

A way of finding the importance flux guess is when the source and the detector are switched. To accomplish this, the point source is moved to the position $(x = 15, y = 15, z = 15)$. The mean values and β-values are calculated using the same principles, see Fig. 5.10 for the results. These β-values will push the correctons into the direction to the detector region. Using the Eq. 5.10, the adjoint flux guess can be loaded into the same model as the discrete guess.

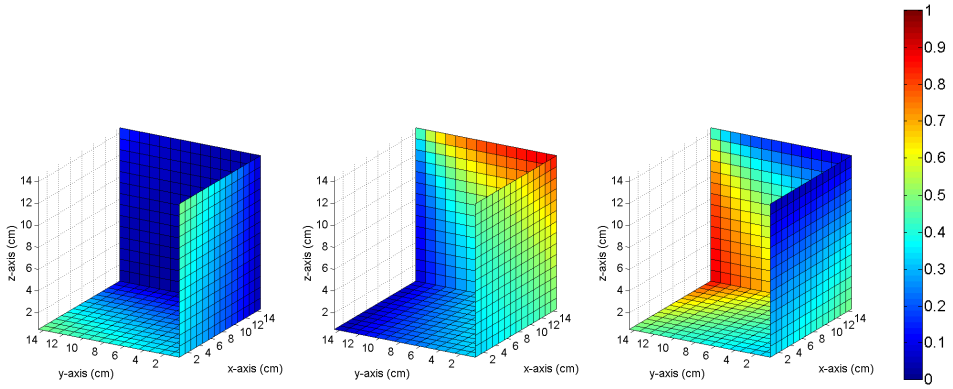

(a) x-direction (b) y-direction (c) z-direction

Figure 5.10: The different β-values in each direction after "normalization".

5.2.2 The Results

Adjoint Flux Guess only with the Discrete Values

The same is done as the discrete flux guess, first the guess is made by only using the discrete values of the adjoint flux guess. The found neutron flux can be seen in Fig. 5.11. The result have the same shape as the result in Fig. 5.3.

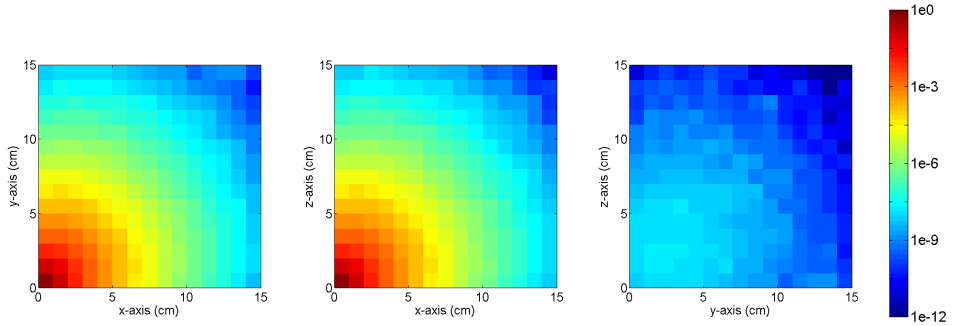

(a) z-plane (b) y-plane (c) the rear side

Figure 5.11: The neutron flux calculated using the discrete values of the adjoint flux guess.

Also the FOM, Fig. 5.12, is similar to Fig. 5.4. The reason for this is that the flux guess looks the same as the flux guess of the discrete value of the discrete guess.

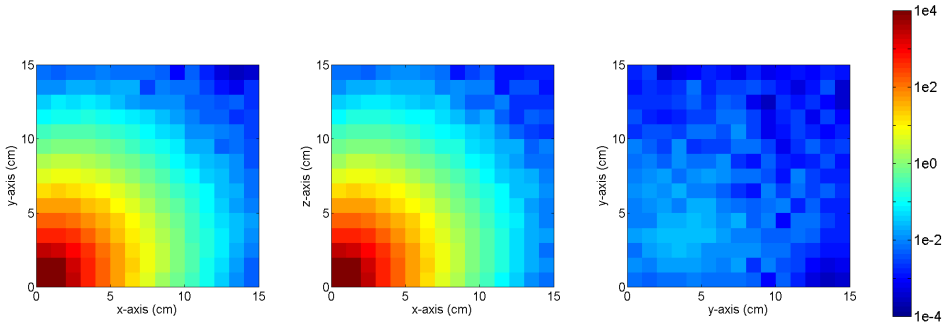

(a) z-plane (b) y-plane (c) the rear side

Figure 5.12: The FOM calculated using the discrete values of the adjoint flux guess.

Adjoint Flux Guess

When adjoint flux guess is used as estimator the found neutron flux, see Fig. 5.13, shows a promising start, because the found neutron flux is not blocky.

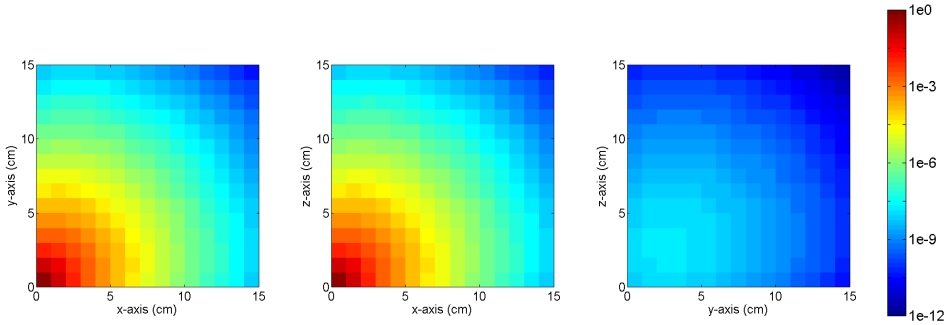

(a) z-plane (b) y-plane (c) the rear side

Figure 5.13: The neutron flux calculated using the adjoint flux guess.

But it the interesting part is found in the FOM of the adjoint flux guess, Fig. 5.14. The FOM-values are relative higher than other techniques, meaning that the calculation is preforming well. The reason why there is no clear tendency seen around the source as in Fig. 5.6 is because the β-values are not that different from each other. The effect of the using adjoint flux guess is seen in Fig. 5.14(c), because at the bottom right the FOM is lower caused by undersampling.

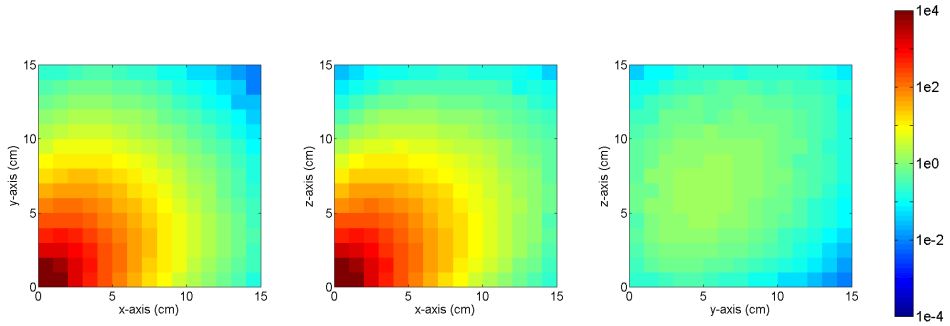

(a) z-plane (b) y-plane (c) the rear side

Figure 5.14: The FOM calculated using the adjoint flux guess.

5.2.3 Comparison of the Found Results

Just like the previous comparisons a closer look is taken at the space diagonal. In Fig. 5.15 the neutron flux and the two flux guesses are plotted. These flux guesses do not have the same shape as Fig. 5.7. At a close look it is seen that the curvature is now a different shape.

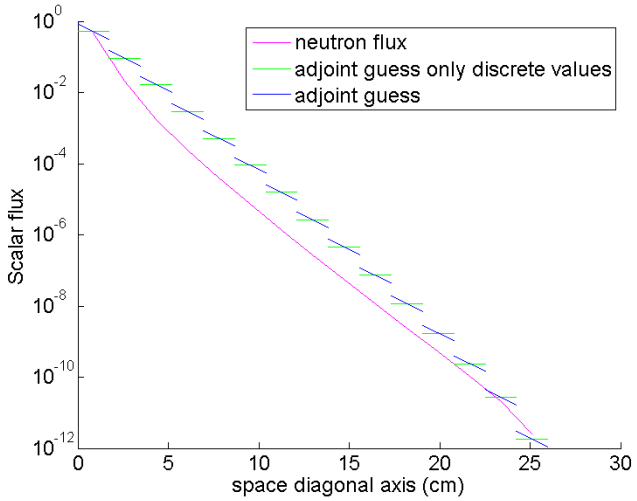

Figure 5.15: An overview of the adjoint flux guess with only discrete values, adjoint flux guess and the found neutron flux.

In Fig. 5.16 the neutron flux is plotted, the discrete values is preforming well but the last data points the found neutron flux are fluctuating, due to undersampling of the bins. This is effect is caused by undersampling of the data points. The adjoint flux guess is preforming good, this is clearly seen in Fig. 5.17.

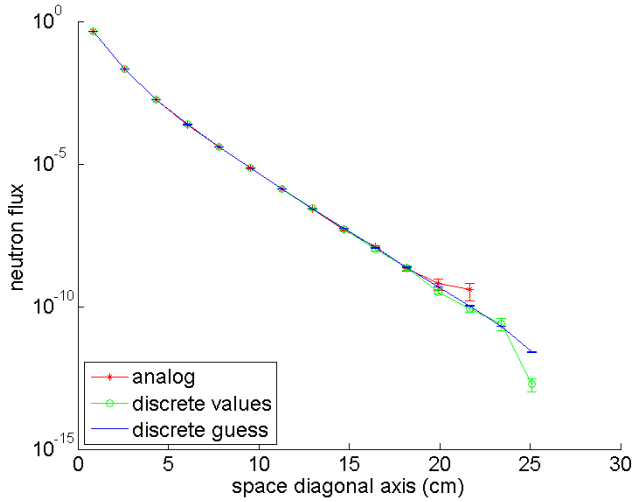

Figure 5.16: The neutron flux calculated with the adjoint flux guess with only discrete values, adjoint flux guess and analog Monte Carlo method.

The FOM of the adjoint flux guess is much higher than the analog and discrete values. The discrete values of the adjoint scalar flux has the same effect as the discrete values of discrete guess. The adjoint flux guess ensures that the particles are the tendency to move to the detector, hence the higher FOM.

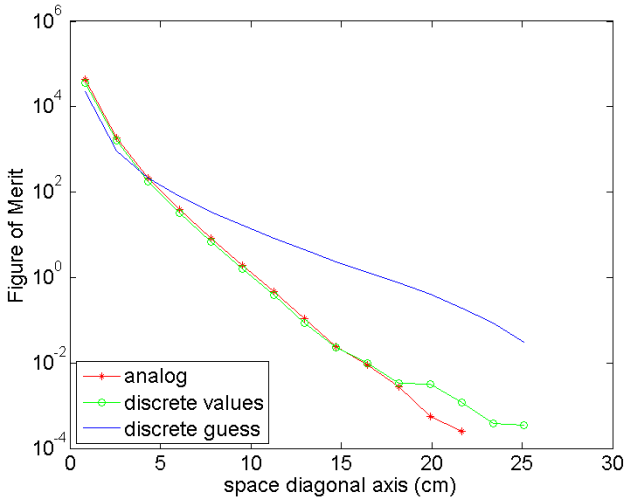

Figure 5.17: The FOM of the adjoint flux guess with only discrete values, adjoint flux guess and analog Monte Carlo method.

5.3 Discrete Flux Guess versus Adjoint Flux Guess

Just like the continuous flux guesses the discontinuous flux guesses are compared by looking at the furthest cell from the source. The data is shown in tables 5.1.

Table 5.1: An overview of the results of the discrete scalar flux guesses in the opposite corner cell in comparison to the source. Where d.f.g. means discrete flux guess and a.f.g. means adjoint flux guess.

Method	FOM	Time needed	Variance	Number of particles
Dimension	–	Hours	$\#^2\text{cm}^{-6}\text{s}^{-1}$	#
Analog	n.a.	2.8	n.a.	10^9
Discrete values of the d.f.g.	$1.853 \cdot 10^{-4}$	3.6	$4.501 \cdot 10^{-24}$	10^9
Discrete guess	$2.673 \cdot 10^{-2}$	4.8	$7.321 \cdot 10^{-24}$	10^9
Discrete values of the a.f.g.	$3.429 \cdot 10^{-4}$	3.4	$3.714 \cdot 10^{-26}$	10^9
Adjoint guess	$2.984 \cdot 10^{-2}$	4.6	$7.185 \cdot 10^{-24}$	10^9

The discrete values of both flux guesses have the same order of FOM, but it is the adjoint discrete values are better preforming with respect to discrete values of the discrete guess. Also the adjoint flux guess is preforming better than the discrete flux guess.The discrete values of the adjoint flux guess has the lowest variance, but when Fig. 5.16 is investigated the found neutron flux shows a large drop at the end, which is not seen before, whereby the relative error is not decreasing, this effect is cause by undersampling.

5.4 Comparison of the Important Techniques

At last the FOMs of the important flux guesses and the analog Monte Carlo method along the space diagonal are plotted in Fig. 5.18. They can be also found separately in Fig. 4.16, 4.18, 5.9 and 5.17 as well those who are not plotted in this figure. The weak estimations of the 1- and 3-directional continuous flux guesses are preforming worst than their strong counterparts and therefore they are not very interesting to see. The same applies for discrete values of the discrete guess, this guess looks a lot like the discrete values of the adjoint guess, but its performance is worse.

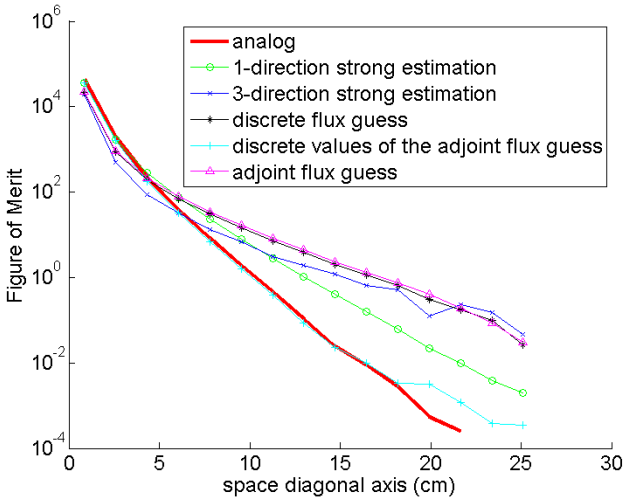

Figure 5.18: The FOM of all important flux guesses and the analog Monte Carlo method.

Three techniques are preforming much better than the analog Monte Carlo method. The strong 3-direction continuous flux guess is preforming the best, but it can not be compared with the discrete flux guess and adjoint flux guess due to the fact that they need more calculation steps. The adjoint flux guess is the best performing discontinuous flux guess.

Chapter 6

Conclusions and Future Directions

Conclusions

The first part of this bachelor project existed of the reproduction of the correcton method in $1D$ space as proven by Becker, [Becker et al, 2006], and Sjenitzer, [Sjenitzer, 2009]. The same results as Becker and Sjenitzer are found, namely that the correcton method preforming better than the analog Monte Carlo Simulation .

The second part was to extend the correcton method to $3D$ space and try different type of scalar flux guesses. The guesses are compared by looking at the FOM. First an analog Monte Carlo simulation is run to see its performance, it has a lot of trouble of penetrating the system. When using a billion particles, the deep parts were not reached and therefore the neutron flux could not be found. All the flux guesses are done using the same number of particles as the analog Monte Carlo method.

At first an 1-directional continuous flux guess is made, two types of guesses are made: a strong and a weak estimation. The weak estimation is able to penetrate the whole system, but when the stronger estimation is used the results are even better. The particles have now the tendency to move into one direction, this is visible in the $2D$ figures of the FOM.

The next step is to use a 3-directional continuous flux guess, where the same decay factor is chosen for each direction. These flux guesses have lower maximum value for the decay factor as the 1-directional flux guess, due to the sum of the angles. Here is also chosen for a weak and strong estimation. The weak estimation is better preforming than the strong estimation of the 1-directional flux guess. When a stronger estimation is used the FOM becomes higher.

The following move is use discontinuous flux guesses. With the use of diffusion theory a discrete guess is made. This guess is used in two ways, first with only the discrete values and discrete values with the found decay factors (discrete guess). The discrete values will extend the lifetime of the particles, but the deeper parts of the system are still under sampled. When the discrete guess is used the FOM-values are higher through out the system.

The last investigated flux guess is the adjoint flux guess, this guess uses an importance function. The adjoint flux guess gives the particles a tendency to move to a certain point. This leads to the fact that this point will have increase of sampling, hereby the variance will decrease. The results are that the discrete values of adjoint flux preforming better than the discrete values of the discrete flux guess. The adjoint flux guess was the best behaving discontinuous flux guess.

The continuous and discontinuous flux guesses can not be compared due to the fact that the discontinuous flux guess needs more calculation between the collisions. For this system the 3-directional continuous flux guess recommend, because the calculation steps for a new collision position are done quick and the FOM has the highest score. When a more complex system is used the adjoint flux guess is recommended, because the adjoint flux guess is almost scoring the same FOM despite the more calculation steps that are needed. Also it is easier to implement different material properties throughout the system.

Future Directions

There are several things that can be investigated in future research. For instance the limits of the decay factors of the discontinuous flux guess are probably higher than assumed, because the sum of the decay factors in the continuous flux guess are higher than the maximum value of the discontinuous flux guess. When the decay factor can be chosen higher the flux guesses will be preforming better, just like the difference between the weak and strong estimations of the continuous flux guesses.

The discrete and the adjoint flux guess might be better determined by using an deterministic code. In this way better β-values can be found which will decrease the variance in the system.

An other aspect that can be changed is the material properties of the system. Instead of only using an absorber, a reflector and/or fissile material can be added to the system, but also a combination of materials can be used. But likewise the scattering can be biased or a biased correcton method can be used as proposed by Becker, [Becker et al, 2006].

To achieve a more homogeneous distribution throughout the system one could think of using weight windows. In this way any outliers will be removed making the calculation more accurate.

The last thing that might be interesting is a self-learning algorithm, which will performance better after each time the code is run.

Acknowledgements

I would like to thank Bart Sjenitzer very much for his excellent guidance during the project and very useful discussions that helped me write this report. Also I would like to thank Bart for times he help to debug the code. Furthermore I would like to thank the entire PNR group for the great time I had during the project.

Bibliography

Becker et al, 2006
T.L. Becker, A.B. Wollaber and E.W. Larsen. *A Hybrid Monte Carlo-Deterministic Method for Global Particle Transport Calculations.* University of Michigan, 2006, cited at page 155-167

Becker, 2009
T.L. Becker. *Hybrid Monte Carlo/Deterministic Methods for Radiation Shielding Problems.* University of Michigan, 2009, cited at page 65-67

Dekking et al, 2003
F.M. Dekking, C. Kraaikamp, H.P. Lopuhä and L.E. Meester. *Kanstat, Probability and Statistics for the* 21^{st} *Century.* TU Delft University Press, 2003, cited at page 18.

Duderstadt et al, 1976
James J. Duderstadt and Louis J. Hamilton. *Nuclear Reactor Analysis* John Wiley & Sons, 1976, cited at page 16-18, 21, 75, 76, 81.

Hoogenboom et al, 2008
J. Eduard Hoogenboom and Stavros Christoforou. *Lecture slides Nuclear Physics, Special topics* TU Delft, 2008, cited at lecture 3

Jäckel et al, 2010
Peter Jäckel and Eckhard Platen. *Encyclopedia of Quantitative Finance, chapter Monte Carlo Simulation* Wiley, 2010.

Lathouwers et al, 2010
Danny Lathouwers and Jan Leen Kloosterman. *Lecture slides Nuclear Reactor Physics* TU Delft, 2010, cited at lecture 2 (slide 2)

Sjenitzer, 2009
Bart Sjenitzer. *Variance reduction using the correcton method on criticality calculations* TU Delft, 2009, cited at 10, 13-15, 18-20